THESIS

STRONG AND WEAK COLD POOL COLLISIONS

Submitted by

Nicholas Michael Falk

Department of Atmospheric Science

In partial fulfillment of the requirements

For the Degree of Master of Science

Colorado State University

Fort Collins, Colorado

Spring 2022

Master's Committee:

Advisor: Susan C. van den Heever

Russ S. Schumacher
Subhas K. Venayagamoorthy

ABSTRACT

STRONG AND WEAK COLD POOL COLLISIONS

Collisions between convective cold pools commonly initiate new convective storms. This occurs through enhancements to the vertical velocity through mechanical forcing, and increased water vapor content via thermodynamic forcing. The goal of this study is to investigate the impact of the following four parameters on the mechanical and thermodynamic forcing associated with cold pool collisions: (1) the initial temperature perturbation of cold pools, (2) the initial distance between cold pools, (3) the environment in which cold pools exist, and (4) the strength of atmospheric diffusion. To achieve this goal, the dynamical and thermodynamical processes of colliding pairs of cold pools is investigated using a two-dimensional, high-resolution non-hydrostatic anelastic model. The four parameters of interest were varied across a wide range of values in a model suite comprised of 11,200 large eddy simulations in total. To facilitate our analysis, a classification of cold pool collisions into categories of "mechanically strong" and "mechanically weak" is proposed. "Mechanically strong" cold pool collisions occur when the updraft velocities resulting from the collisions are greater than those produced by the flow of air forced up the leading edges of individual cold pools. In "mechanically weak" collisions, the updraft velocities produced by individual cold pools are greater than those from cold pool collisions. An analogous classification of "thermodynamically strong/weak" collisions is also proposed.

The results of this analysis show that the initial temperature perturbation of the cold pools has the largest impact on mechanical and thermodynamic forcing from cold pool collisions.

Colder cold pools have greater horizontal wind velocities at their heads, leading to greater near-surface horizontal convergence when they collide. This in turn leads to greater updraft velocities which are also more effective at advecting water vapor upwards. The second largest impact on mechanical and thermodynamic cold pool forcing is from the environment in which the cold pools exist. Due to a decreased vertical gradient of potential temperature, weaker low-level static stability increases mechanical forcing as the air lofted by the collisions is decelerated less by negative buoyancy. Environments with larger low-level vertical moisture gradients are associated with increased thermodynamic forcing through enhanced vertical moisture advection.

The initial edge-to-edge distance between the cold pools has the third largest impact on the proxies for convective initiation. Mechanical forcing is found to peak at an optimal initial distance between cold pools of ~2.5 km due to a balance between the creation and dissipation of kinetic energy. Thermodynamic forcing, on the other hand, peaks for much greater initial cold pool distances than those associated with the mechanical forcing. This is likely a result of the faster updraft winds generated during collisions for closely spaced initial cold pools also being more effective at advecting moisture away during the collision, thereby decreasing the thermodynamic forcing. The smallest impact on the proxies for convective initiation comes from the atmospheric diffusion rate which impacts cold pool strength through mixing. Thus, this work finds that convective initiation becomes increasingly likely from a cold pool collision when the cold pools are colder, the environment is less stable and has a greater vertical water vapor gradient, the cold pools start close to some optimal separation distance, and the atmospheric diffusion rate is low.

ACKNOWLEDGEMENTS

I am highly fortunate for extraordinary people who have all contributed greatly to the completion of this thesis. I must first thank my advisor, Dr. Susan van den Heever, who has taught me not only much about atmospheric science, but has also contributed deeply to my maturation as a scientist through her mentorship. I greatly appreciate the leeway Sue granted me with this research, and her insightful comments which have fundamentally improved this work. I am grateful to Dr. Russ Schumacher and Dr. Karan Venayagamoorthy for serving on my master's committee. I wish to thank the entire faculty of the CSU Atmospheric Science department for their efforts in teaching highly informative courses. The department staff also deserves many thanks for their assistance with administrative or IT issues, which they always resolve efficiently. I also thank the Atmospheric Science faculty at UC Davis, specifically Dr. Ian Faloona, Dr. Adele Igel, and Dr. Matthew Igel, for preparing me so well for graduate school. I must thank the past and present van den Heever group, Steve Saleeby, Alex Sokolowsky, Ben Ascher, Sean Freeman, Dr. Ross Heikes, Bee Leung, Dr. Leah Grant, Christine Neumaier, Kristen Van Valkenburg, Dr. Bowen Pan, Dr. Emily Riley Dellaripa, Dr. Minnie Park, Brianna Lund, Dr. Yasutaka Murakami, Dr. Jennie Bukowski, Dr. Peter Marinescu, and Dr. Aryeh Drager, for their support and friendship both in and out of work. I have often looked forward to days of work because I spend my time with a group of such friendly, helpful, and kind people. To my friends both in Fort Collins and far away, I say thank you for the support, friendship, and time spent relaxing. I must thank my family, most of all my parents Meg and Mike, for their everlasting encouragement, love, and support. I thank NASA grant 80NSSC18K0149 and NSF grant AGS-2019947 as well for the generous funding for this research.

TABLE OF CONTENTS

Chapter 1: Introduction

1.1 Density Currents and Cold Pools

Density currents, or gravity currents, are a common phenomenon in many fluids. Such currents form due to differences in density between two fluids or a difference in density within the same fluid, even when such density differences are quite small (Simpson 1997). Thunderstorm outflows, sea-breeze fronts, power station effluence, oil slicks, avalanches, pyroclastic flows, turbidity currents on the ocean floor, and even cold air entering a heated house on a winter day are all examples of density currents. Observations as far back as during the Thunderstorm Project noted the presence of cold outflow from thunderstorms caused by evaporative cooling (Byers and Braham 1949). The outflow of a thunderstorm is alternatively known as a convective cold pool, with the cold pool edge often referred to as an outflow boundary or gust front. Analysis of cold pools and comparison to laboratory tank density current experiments more than 50 years ago led to the understanding that cold pools are density currents (Simpson 1969, Simoson 1972, Charba 1974).

Density currents evolve through three distinct phases, which are described by Huppert and Simpson (1980). The first phase is referred to as slumping, in which the motion of the surrounding fluid slows the propagation of the density current. Using a simple model and tank experiments, Huppert and Simpson (1980) determined the slumping phase ends when the ratio between the depth of the current to the depth of the surrounding fluid is less than 0.075. They derived equations for the propagation of two-dimensional and axisymmetric density currents during the slumping phase, finding a constant propagation rate in both cases. The second phase is the inertial phase, during which the propagation speed of the density current is proportional to

time to the negative third power. During the final viscous phase, viscous forces balance the buoyant force of the density current. Huppert and Simpson (1980) found that if viscous forces begin to dominate before the slumping phase ends, then the viscous phase follows the slumping phase and the inertial phase is skipped.

1.2 Roles of Convective Cold Pools

Convective storms are a ubiquitous feature of the atmosphere (Zipser et al. 2006), and thus so are convective cold pools. Cold pools play several important roles in the atmosphere, one of which is their impact on storm longevity and intensity. During the Thunderstorm Project, it was noted that cold pools can cut off the flow of warm moist air into a storm (Byers and Braham 1949). The storm may then begin ingesting cold, nonbuoyant air from the cold pool, which hastens the dissipation of the storm, a process also noted by Droegemeier and Wilhelmson (1985a). Conversely, in certain situations, cold pools can benefit storm longevity and intensity. Houston and Wilhelmson (2011) found that in low-shear environments the deeper cold pools of quasi-linear convective systems force deeper ascent which supports the storm longevity, whereas initially isolated storms are shorter-lived as their shallower cold pools are insufficient to contribute to the updraft. In higher shear environments, Parker (2007) similarly found that the stronger cold pools of clustered storms promote the longevity of the storms. Wilson and Megenhardt (1997) analyzed data from the Convection and Precipitation/Electrification experiment conducted in July and August 1991 and concluded that understanding the speed and orientation of cold pool gust fronts was critical for forecasting storm lifetime and organization.

Cold pools are also critical to the organization and propagation of convective storms. RKW theory postulates that cold pools play a critical role in organizing and maintaining squall

lines through their interaction with the environmental wind shear (Rotunno et al. 1988, Weisman and Rotunno 2004). When the horizontal vorticity of the cold pool and the environment are in balance, the resulting vertical motion is upright and thus most efficient. When these vorticities do not balance, the resulting updraft motion is tilted and less efficient. While RKW theory is thought to be more applicable in midlatitude environments, as balance between the wind shear and cold pool is more common in such environments, some studies argue that cold pools are actually detrimental to organized convective systems in the tropics. Grant et al. (2018) found that in low shear tropical environments that storms were weakened by ingesting negatively buoyant cold pool air. Grant et al. (2018) argued that gravity waves, not cold pools, played the key role in organizing the simulated systems.

Cold pools can also initiate new convective storms. Goff (1976) noted that cold pools can lift moist environmental air at their edges thereby producing clouds. This lifting can lead to the eventual formation of new deep convection at the cold pool edge (Purdom 1982, Wilson and Schreiber 1986, Weckwerth and Wakimoto 1992). Mechanical forcing (Droegemeier and Wilhelmson 1985a,b) and thermodynamic forcing (Tompkins 2001) have been identified as two mechanisms by which convective initiation from cold pools can occur (Torri et al. 2015). Mechanical forcing refers to the creation of new convection by the process of lifting environmental air up and over the cold pool edge, or gust front, so that it reaches the environmental level of free convection (LFC) (Purdom 1976, Weaver and Nelson 1982, Droegemeier and Wilhelmson 1985a,b, Meyer and Haerter 2020). Thermodynamic forcing, on the other hand, refers to an increase in the water vapor mixing ratio at the cold pool edge which subsequently lowers the LFC (Tompkins 2001, Feng et al. 2015, Langhans and Romps 2015). This enhanced water content decreases the amount of lifting needed to initiate convection and

thus increases the likelihood that convection will occur. Recent research shows that cold pools increase the water vapor mixing ratio at their edges primarily through increased latent heat fluxes (Langhans and Romps 2015), but that advection of preexisting moisture and evaporation of precipitation may also contribute to this increase in a non-negligible way (Schlemmer and Hohenegger 2016, Torri and Kuang 2016). Tompkins (2001) noted in a numerical simulation of a tropical environment that new convection was triggered by mature cold pools with negligible mechanical lifting but substantial increases in water vapor mixing ratio, and argued that thermodynamic forcing was more important than mechanical forcing in the tropics. However, Torri et al. (2015), who conducted simulations in a similar idealized tropical oceanic environment to Tompkins (2001), suggested that both thermodynamic and mechanical forcing play an important role in generating new convection in such an environment. Thus, there is still much to be understood about these two forms of cold pool forcing. Collisions between cold pools, can also initiate convection; this phenomenon is discussed further in chapter 1.3.

Surface fluxes can also be impacted by cold pools, and vice versa. Tompkins (2001) found that surface sensible and latent heat fluxes were enhanced inside of tropical oceanic cold pools due to their enhanced winds, lower water vapor content, and colder temperatures, and including of cold pool-induced surface fluxes in a simulated oceanic squall line was found to decrease cold pool area (Trier 1996). Grant and van den Heever (2018) argued that including two-way fluxes between the cold pool and the land surface is critical to representing cold pool properties correctly. They compared two simulated cold pools, one simulation having interactive land surface fluxes and the other having prescribed fluxes, and found that the cold pool in the former case dissipated twice as fast and covered half the area due to enhanced sensible heat fluxes near the cold pool edge. Surface fluxes may not always serve to dissipate cold pools.

Simulations conducted by Drager and van den Heever (2017) found strong evaporative cooling on the surface can lead to negative surface sensible heat fluxes which act to strengthen cold pools. Bukowski and van den Heever (2021) found negative sensible heat fluxes in haboobs due to longwave radiation causing air to warm faster than the surface during the transition from day to night.

Finally, convective cold pools plan in important role in the transport of aerosols including dust and pollen, and may also generate severe weather hazards. In some situations, cold pools can increase the concentration of atmospheric aerosols via by enhancing the lofting of aerosols from the surface. Observations in Colorado have shown cold pools can increase ice nucleating particle concentrations by an order of magnitude (Langer et al. 1979). Dust storms formed by cold pools, also known as haboobs, can contribute up to 30% of atmospheric dust production on a regional scale; haboobs are also major public health and aviation hazards (Miller et al. 2008). Regardless of lofted dust or pollen, cold pools can also be a major hazard at the surface due to damaging winds they create and to aircraft due to the intense turbulence associated with cold pools (Simpson 1997).

1.3 Convective Initiation by Cold Pool Collisions

Convective storms can have large impacts on life and the economy. For example, 3,000-5,000 fishermen die every year on Lake Victoria due to thunderstorms (Thiery et al. 2016) and individual thunderstorms in Colorado can cause millions of dollars of crop loss (Childs et al. 2020). Understanding how cold pool collisions can trigger these storms is therefore critical.

Collisions between cold pools can enhance lifting compared to that of individual cold pools and similarly initiate new convection (Droegemeier and Wilhelmson 1985a,b). Since the

detection of near-surface lifting is important for forecasting convective storms (McNulty 1995), understanding more about how cold pool collisions initiate convection is critical. Furthermore, convective initiation by cold pool collisions is a regular occurrence in the atmosphere. Wilson and Schreiber (1986) noted that collisions between boundary layer convergence lines, often the edges of cold pools, enhanced an existing storm or initiated a new storm 84% of the time. In the southwest Amazon on a day with minimal synoptic forcing, it was also found that 52% of storms were initiated from cold pools with 36% initiating from non-colliding cold pools and 16% from colliding cold pools (Lima and Wilson 2008). The focus of this work is therefore on the important and relatively frequent phenomenon of convective initiation by colliding cold pools.

Droegemeier and Wilhelmson (1985a,b) investigated convective initiation from cold pool collisions in a numerical model and noted that the air was "literally squeezed out" of the space between the cold pools, thereby creating lifting and storms upshear and downshear of the line connecting the initial warm bubbles. Analysis of three colliding cold pool case studies in Colorado found that in each case the warmer cold pool was lifted to sufficient heights over the colder cold pool to initiate convection (Intrieri et al. 1990). Kingsmill (1995) analyzed a case of a cold pool colliding with a sea breeze front in Florida. He found that updraft intensities were similar before and after the collision, and thus convective activity was not enhanced by the collision.

Several recent numerical modeling studies have further investigated cold pool collisions. One study using a high-resolution case-study model simulation to investigate colliding cold pools found that colliding cold pools were larger (due to the cold pools merging), more negatively buoyant, and moistened the environment more than isolated cold pools (Feng et al. 2015). Torri and Kuang (2019) demonstrated that cold pools in tropical maritime regions tend to

be clustered and often collide within 10 minutes of forming. Their RCE simulations also showed that cold pool collisions deform cold pools into non-circular shapes, and argue that collisions are a key dynamical process of cold pools. Meyer and Haerter (2020) (hereafter MH20) tested two-cold pool collisions and three-cold pool collisions in dry, uniform environments without wind shear. They showed that two-cold pool collisions created larger vertical velocities than the collisions between three cold pools, but that three-cold pool collisions created more total updraft mass flux. They also noted that collision-induced updrafts are shallower in statically stable environments compared with statically neutral environments, and that cold pools that start further apart produce smaller peak vertical velocities later in the simulation.

Liu and Moncrieff (2000) and Seigel and van den Heever (2012) showed that the strength and vertical profile of stability can greatly affect the propagation of individual cold pools. Liu and Moncrieff (2000) noted that there are three ways in which low-level static stability influences cold pools. Firstly, a stabilization effect in which the vertical gradient in potential temperature in a statically stable environment leads to parcels that are lifted upward having lower potential temperature than surrounding air. Thus, these lifted parcels are negatively buoyant. This negative buoyancy acts to oppose the lifting and becomes more forceful as static stability increases (Liu and Moncrieff 2000). Secondly, an adiabatic cooling mechanism in which mechanically lifted ambient air affects the horizontal pressure gradient and can increase or decrease the propagation speed of cold pools. Finally, the radiation of energy by gravity waves slows down cold pools in continuously stratified environments and environments with deep stable stratification above neutral stratification. Expanding on this research, Siegel and van den Heever (2012) found that cold pools in environments with shallow stable stratification on top of neutral stratification do not slow down if the stable layer is shallow enough to avoid acting as a

gravity wave ducting layer. The impacts of such environmental stability effects should be investigated for colliding cold pools.

The goal of this study is to investigate the sensitivity of cold pool collisions and the subsequent initiation of moist convective updrafts to several parameters including: (1) the initial temperature perturbation of the cold pools; (2) the initial distance between the cold pools; (3) the strength of the diffusion; and (4) the background environments in which cold pools form. The relative impact of each parameter will also be explored. It is anticipated that collisions between colder cold pools will produce the greatest proxies for convective initiation, but that this will be modulated by the environment in which they form, and by how much the cold pools are dissipated by the time they collide, which in turn will depend on the initial distance between the cold pools and the diffusion strength. This study therefore extends the study by MH20. While MH20 tested two different dry idealized environments, a number of different environments that range from dry idealized environments to realistic midlatitude and tropical environments with moisture are investigated here. In addition, the roles of the initial temperature perturbation of the cold pools and the diffusion strength in cold pool collisions are also analyzed. The parameter space is examined thoroughly through the use of 11,200 total idealized simulations. Chapter 2 describes the model setup and experimental design of these simulations. The dynamics and thermodynamics of a cold pool collision are examined in chapter 3. Chapter 4 discusses the effects of the tested parameters on cold pool collisions. Conclusions of this work are finally presented in chapter 5.

Chapter 2: Methods

2.1 LES Model Setup

Simulations were run using a high resolution non-hydrostatic anelastic large eddy simulation (LES) model run in two dimensions. Such models have been found to be a useful tool for investigating cold pools (Liu and Moncrieff 1996, Liu and Moncrieff 2000, Seigel and van den Heever 2012, Grant and van den Heever 2016). While three-dimensional models perform better in capturing some of the processes important for cold pools, such as the breakdown of Kelvin-Helmholtz waves (Grant and van den Heever 2016), the computational expediency of two-dimensional simulations allows for large numbers of simulations to be run at higher grid resolutions, and hence for a more thorough exploration of the associated parameter spaces.

The model utilized for this study solved the following equations

$$\frac{\partial u}{\partial t} = -\frac{\partial uu}{\partial x} - \frac{1}{\bar{\rho}}\frac{\partial \bar{\rho} uw}{\partial z} - c_{p_d}\overline{\theta_v}\frac{\partial \pi'}{\partial x} + K_{mx}\frac{\partial^2 u}{\partial x^2} + K_{mz}\frac{\partial^2 u}{\partial z^2} \quad (1)$$

$$\frac{\partial w}{\partial t} = -\frac{\partial uw}{\partial x} - \frac{1}{\bar{\rho}}\frac{\partial \bar{\rho} ww}{\partial z} - c_{p_d}\overline{\theta_v}\frac{\partial \pi'}{\partial z} + g\left(\frac{\theta'}{\bar{\theta}} + 0.61 r_v'\right) + K_{mx}\frac{\partial^2 w}{\partial x^2} + K_{mz}\frac{\partial^2 w}{\partial z^2} \quad (2)$$

$$\frac{\partial \theta'}{\partial t} = -\frac{\partial u\theta'}{\partial x} - \frac{1}{\bar{\rho}}\frac{\partial \bar{\rho} w\theta'}{\partial z} - w\frac{d\bar{\theta}}{dz} + K_{hx}\frac{\partial^2 \theta'}{\partial x^2} + K_{hz}\frac{\partial^2 \theta'}{\partial z^2} \quad (3)$$

$$\frac{\partial \pi'}{\partial t} = -\frac{\bar{c}_s^2}{\bar{\rho} c_{p_d}\overline{\theta_v}^2}\left(\bar{\rho}\overline{\theta_v}\frac{\partial u}{\partial x} + \frac{\partial \bar{\rho}\overline{\theta_v} w}{\partial z}\right) + K_{hx}\frac{\partial^2 \pi'}{\partial x^2} + K_{hz}\frac{\partial^2 \pi'}{\partial z^2} \quad (4)$$

$$\frac{\partial r_v'}{\partial t} = -\frac{\partial u r_v'}{\partial x} - \frac{1}{\bar{\rho}}\frac{\partial \bar{\rho} w r_v'}{\partial z} - w\frac{d\overline{r_v}}{dz} + K_{hx}\frac{\partial^2 r_v'}{\partial x^2} + K_{hz}\frac{\partial^2 r_v'}{\partial z^2} \quad (5)$$

using the leapfrog scheme in time and centered differencing in space. Overbars represent environmental values for variables while primes represent perturbations from these environmental values, where u is the horizontal component of the wind velocity vector, w the vertical component of the wind velocity vector, θ the potential temperature, r_v the water vapor

mixing ratio, C_{p_d} the heat capacity of dry air, g the acceleration due to gravity, $\overline{c_s}$ the speed of sound, K_{mx} and K_{mz} the eddy diffusion coefficients for winds, and K_{hx} and K_{hx} the eddy diffusion coefficients for scalars. Exner function π is given by the following equation

$$\pi = \left(\frac{p}{p_0}\right)^{\frac{R_d}{C_{p_d}}} \tag{6}$$

for pressure p, reference pressure $p_0 = 1000\ hPa$, and dry air gas constant R_d.

The 2D Arakawa C grid used was 803 points by 160 points in the horizontal (x) and vertical directions (z), respectively. Sensitivity tests using a grid three times the size in the horizontal (2409 points), yielded maximum vertical velocities and water vapor mixing ratios that differed by less than 1.4% from the grid with 803 points. Grid spacings of 100 m in the horizontal and 50 m in the vertical were chosen as such spacings have been shown to be necessary to accurately represent cold pool processes (Grant and van den Heever 2016). The timestep was 0.25 s. A Robert-Asselin filter was applied using gamma of 0.2. A Rayleigh damping layer was implemented in the uppermost 300 m of the model domain with a timescale of 60 s to avoid reflection of gravity waves off the model top. Periodic lateral boundaries were applied. Full-model output was saved every minute, while domain maximum vertical velocity, domain maximum absolute value of horizontal wind, and domain minimum potential temperature were saved every timestep. While water vapor was present in the model, water vapor was not allowed to condense, and no other microphysical processes were accounted for. The effects of water vapor on buoyancy were included, and water vapor was allowed to advect and diffuse around the domain. All of the model settings used to conduct these experiments are summarized in Table 2.1. The cold pools were initiated using cosine smoothed bubbles centered at the surface with vertical radii of 1000 m and horizontal radii of 2500 m. Two cold pools were initiated at a specified distance apart in each simulation and allowed to subsequently collide.

2.2 Experimental Design

Sixteen suites of sensitivity experiments were conducted. Each suite included simulations in which the initial minimum potential temperature perturbation (hereafter initial temperature perturbation) of the cold pools was varied from -1 K to -20 K at intervals of 1 K (20 values), and the initial edge-to-edge distance (hereafter initial distance) of the cold pools was varied from 0 m to 27200 m at intervals of 800 m (35 values). Note that while the temperature perturbations in cold pools are negative, further mentions of cold pool temperature perturbations in this text will omit the negative sign for clarity. All combinations of these two parameters were tested for a total of 700 simulations per experiment suite. The range of initial temperature perturbations was chosen based on the analysis of the Oklahoma Mesonet data conducted by Engerer et al. (2008) which showed coldest cold pool temperature perturbations of 17 K, and observations of cold pools in tropical environments which may have temperature perturbations less than 1 K (Tompkins 2001). MH20 tested initial distances of 10, 12, and 15 km. This study tested the closest initial distance possible (0 m), for the sake of completeness, up to almost 2 times HM20's tested maximum (27200 m). Beyond this distance, collisions between even the coldest initial cold pools did not produce vertical velocities greater than those produced by the preliminary spreading of the cold pools in the first experiment suite that was run (which was the WK suite, see the next paragraph for details). The model suites differ only in their base-state environment and/or their eddy diffusion coefficients. Table 2.2 summarizes the 16 different experiment suites, lists their nomenclature, and groups them by idealized (IDEAL), continental (CONT), and tropical (TROP) environments.

The standard eddy diffusion coefficient values used were $K_{mx} = 50\ m^2\ s^{-1}$, $K_{mz} = 25\ m^2\ s^{-1}$, $K_{hx} = 150\ m^2\ s^{-1}$, and $K_{hz} = 75\ m^2\ s^{-1}$, which are the same as those used by

Grant and van den Heever (2016) for their simulations with grid spacings of 100 m in the horizontal and 50 m in the vertical. Experiments designated “Halved (Doubled) K’s” used half (double) these standard coefficients. Cold pools in simulations with increased (decreased) eddy diffusion coefficients are expected to dissipate faster (slower) compared to cold pools in simulations with the standard eddy diffusion coefficient values. Cold pool lifetimes, and thus dissipation rates, can vary wildly across environments. Feng el al. (2015) observed cold pools over the tropical ocean and noted many cold pools lasting only 1-2 hours, while Roberts and Knippertz (2012) noted a Saharan cold pool which lasted nearly 2 days. Thus, varying the eddy diffusion coefficients was used as a simple way to test the effect of the rate at which cold pools dissipate on convective initiation from cold pool collisions.

Figure 2.1 shows Skew-T log-p diagrams of the 8 different tropical, midlatitude and isentropic environments tested. No base state wind was used in any experiment, as the goal of this study is to investigate symmetric cold pool collisions. The dry isentropic environment (DI) had no water vapor and a constant potential temperature of 300 K throughout. This option was selected to obtain results in an environment without static stability that can subsequently be compared with results from the remaining environments that do include levels with static stability. Additionally, dry isentropic environments are commonly used in idealized cold pool modeling studies (Liu and Moncrieff 2000, Seigel and van den Heever 2012, Meyer and Haerter 2020). The nocturnal environment (NT) also included no water vapor and consisted of a layer from 0-1 km with a constant Brunt-Väisälä frequency of 0.01 s^{-1} and was dry isentropic above 1 km. NT is representative of a stable nocturnal boundary layer. The half-stability nocturnal (NT_HS) and double stability nocturnal (NT_DS) environments were identical to NT except for having Brunt-Väisälä frequencies of 0.005 s^{-1} and 0.02 s^{-1} for the 0-1 km layer, respectively.

Thus, DI, NT_HS, NT, and NT_DS provide a set of experiment suites where the static stability was steadily increased from 0 s^{-1} to 0.02 s^{-1}. Liu and Moncrieff (2000) tested individual cold pools in similar environments.

To test an environment representative of atmospheric conditions in the Midwestern US in spring, the Weisman-Klemp environment (WK) suite was run using an environment with the same temperature profile as that of Weisman and Klemp (1982). The dewpoint profile used here, however, is greater just above the surface, but generally lower at the top of the boundary layer and aloft compared to that of Weisman and Klemp (1982). The mid-stability environment used by Sokolowsky et al. (2021), representative of idealized tropical maritime conditions, was tested as the Sokolowsky (SK) environment. Finally, the S07 and S10 environments were taken from two different dropsondes released during the CAMP2Ex field campaign (Reid et al. 2021), specifically science flight 7 sonde 7 and science flight 12 sonde 10, respectively. Both of these sondes were dropped just outside of cold pools over the tropical ocean around the Philippines. As the S07 and S10 sondes were dropped from altitudes lower than the top of the model domain, ERA5 reanalysis was used above 6km to extend the data to the top of the model domain. Linear smoothing with height between ERA5 and the dropsonde data was used between 5 km and 6 km in the S07 and S10 environments to ensure a continuous atmospheric profile. Note that while the SK, S07, and S10 environments are all representative of tropical conditions, SK was from an idealized numerical experiment, while S07 and S10 used observational data. The set of environments tested includes idealized environments in which cold pools are often examined (DI) or are representative of real conditions that cold pools encounter (NT_HS, NT, and NT_DS), including a midlatitude environment conducive to convection (WK), and tropical environments conducive to convection (SK, S07, S10). Thus, the collisions examined here

occurred within a wide range of different environments, from the tropics to the midlatitudes, from continental to maritime, and from idealized to observational, and are therefore representative of the many conditions supporting cold pool development.

The general nomenclature for each experiment follows the format: experiment_abbrevation_Txx_Dyyy where experiment_abbrevation is the abbreviated name of each experiment suite (Table 2.2), xx is the initial temperature perturbation of the simulated cold pools in Kelvin with the negative sign removed, and yyy is the initial distance between cold pools in hectometers (for the sake of simplicity).

2.3 Tables and Figures

Table 2.1: Summary of settings used in the 2D anelastic model to conduct the experiments.

Model Setting	**Value/Type**
Model type	2D anelastic, nonhydrostatic
Timestep	0.25 s
Horizontal Grid Spacing	100 m
Vertical Grid Spacing	50 m
Number of x points	803
Number of z points	160
Simulation duration	1 hour
Data Output frequency	1 minute
Speed of Sound (for anelastic approximation)	50 m/s
Lateral boundary conditions	Cyclic
Surface boundary condition	Freeslip
Rayleigh damping layer depth	300 m
Rayleigh damping layer timescale	60 s
Initial Bubble x Radius	2500 m
Initial Bubble z Radius	1000 m
Initial Bubble Maximum Theta Perturbation	Varies: -1 K to -20 K every 1 K
Initial Distance Between Bubbles	Varies: 0 m to 27200 m every 800 m

Table 2.2: The nomenclature and descriptions for each experiment suite. For each suite, 700 simulations were run in which the initial minimum potential temperature perturbation of the cold pools was varied from -1 K to -20 K at an interval of 1 K, and the initial edge-to-edge distance between the cold pools was varied from 0 m to 27200 m at an interval of 800 m.

Experiment Suite Group	Experiment Suite Long Name	Experiment Suite Abbreviation	Experiment Suite Description
IDEAL	Dry Isentropic	DI	A profile with constant potential temperature of 300 K and no moisture
IDEAL	Dry Isentropic Halved K's	DI_HK	The DI experiment but with eddy diffusion coefficients halved
IDEAL	Dry Isentropic Doubled K's	DI_DK	The DI experiment but with eddy diffusion coefficients doubled
IDEAL	Standard-Stability Nocturnal	NT	A profile with a surface to 1 km deep stable layer with Brunt-Vaisala frequency of 0.01 1/s which is isentropic above 1 km with no moisture, representative of a nocturnal atmosphere over land
IDEAL	Half-Stability Nocturnal	NT_HS	The NT experiment but with the stable layer having a Brunt-Vaisala frequency of 0.005 1/s
IDEAL	Double-Stability Nocturnal	NT_DS	The NT experiment but with the stable layer having a Brunt-Vaisala frequency of 0.02 1/s
IDEAL	Standard-Stability Nocturnal Halved K's	NT_HK	The NT experiment but with eddy diffusion coefficients halved
IDEAL	Standard-Stability Nocturnal Doubled K's	NT_DK	The NT experiment but with eddy diffusion coefficients doubled
CONT	Weisman-Klemp	WK	A profile similar to that used by Weisman and Klemp (1982) which is representative of the Midwestern United States in spring
CONT	Weisman-Klemp Halved K's	WK_HK	The WK experiment but with eddy diffusion coefficients halved
CONT	Weisman-Klemp Doubled K's	WK_DK	The WK experiment but with eddy diffusion coefficients doubled
TROP	Sokolowsky Environment	SK	The mid-stability environment used by Sokolowsky et al. (2020) representative of the tropical ocean surrounding the Philippines
TROP	Sokolowsky Environment Halved K's	SK_HK	The SK experiment but with eddy diffusion coefficients halved
TROP	Sokolowsky Environment Doubled K's	SK_DK	The SK experiment but with eddy diffusion coefficients doubled
TROP	CAMP2Ex SF07 S07 Environment	S07	The profile taken during CAMP2Ex science flight 7 by dropsonde 7, this profile was taken over tropical ocean surrounding the Philippines just ahead of an advancing cold pool
TROP	CAMP2Ex SF12 S10 Environment	S10	The profile taken during CAMP2Ex science flight 12 by dropsonde 10, this profile was taken over tropical ocean surrounding the Philippines just ahead of an outflow boundary

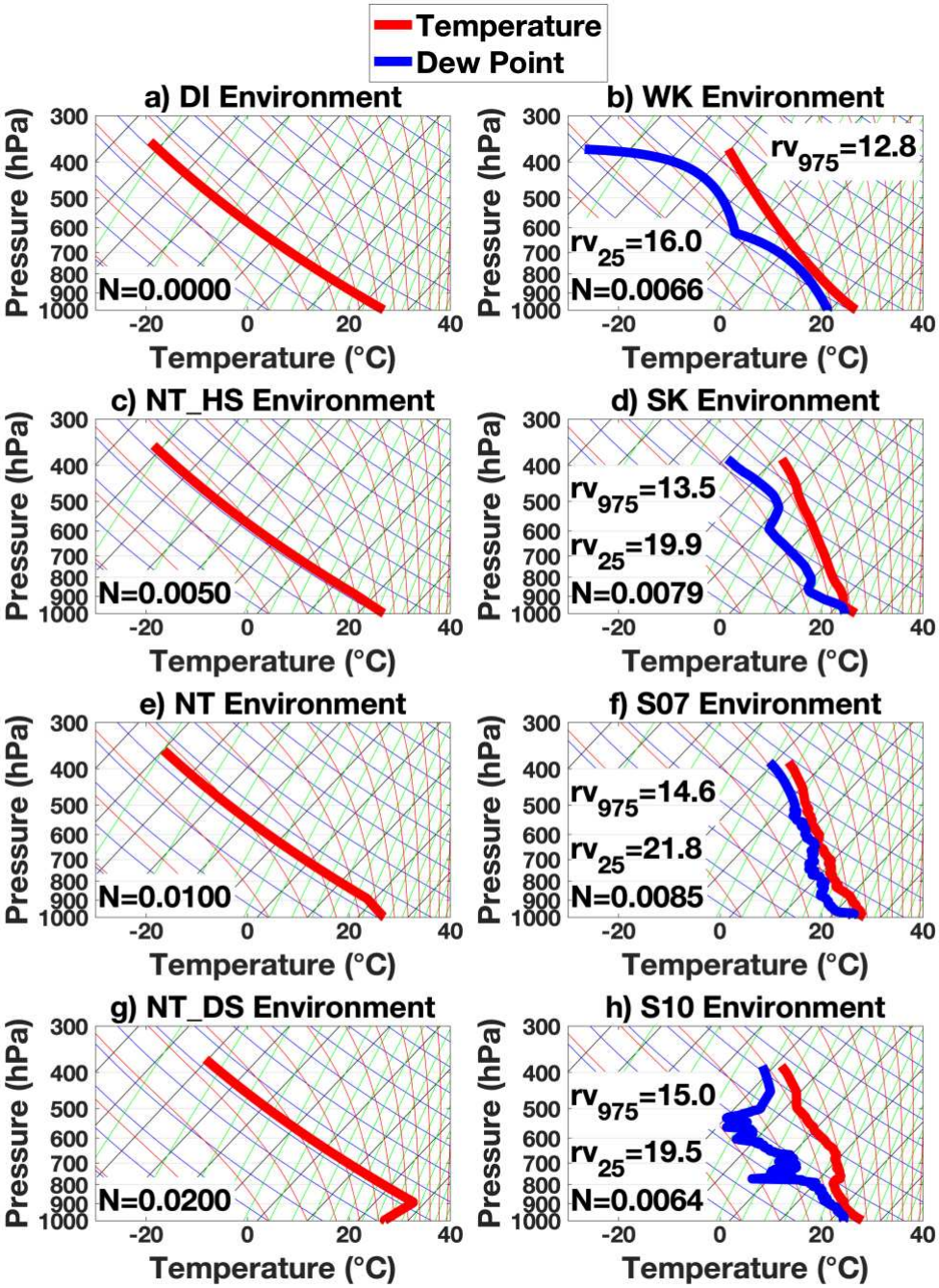

Figure 2.1: Skew-T diagrams for all of the different environments tested. No base state wind was used in any experiment. Each panel lists the water vapor mixing ratio at 975 m (rv_{975}) and 25 m (rv_{25}) for those experiments with moisture in units g kg^{-1}, as well as the Brunt-Väisälä frequency of the 25 m – 975 m layer (N) in units s^{-1}.

Chapter 3: Dynamics and Thermodynamics of a Cold Pool Collision

In this chapter, the WK_T10_D136 (Weisman-Klemp environment, 10K initial temperature perturbation, 13600 m initial distance) simulation is analyzed in detail to describe the physical processes that occur before, during, and after a typical cold pool collision. This simulation is singled out as its initial temperature perturbation of 10 K, and its initial distance of 13600 m between cold pools, are close to the median values tested. The WK experiment suite was chosen as the WK environment has a low-level Brunt-Väisälä frequency of 0.0066 s^{-1}, close to the median value of 0.00725 s^{-1}, and has standard diffusion.

Vertical velocity and water vapor mixing ratio form the focus of the subsequent analysis as enhancements in one or both are critical to convective initiation. The advection of vertical velocity (ADV_W), the vertical buoyancy (BUOY_W), the vertical perturbation pressure gradient force (PRESS_W), and the diffusion of vertical velocity (DIFF_W) are defined as follows:

$$ADV\_W = -\frac{\partial uw}{\partial x} - \frac{1}{\bar{\rho}}\frac{\partial \bar{\rho} ww}{\partial z} \tag{7}$$

$$BUOY\_W = g\left(\frac{\theta'}{\bar{\theta}} + 0.61 r_v'\right) \tag{8}$$

$$PRESS\_W = -c_{p_d}\overline{\theta_v}\frac{\partial \pi'}{\partial z} \tag{9}$$

$$DIFF\_W = K_{mx}\frac{\partial^2 w}{\partial x^2} + K_{mz}\frac{\partial^2 w}{\partial z^2} \tag{10}$$

Using these abbreviations, equation 2 can be rewritten as follows.

$$\frac{\partial w}{\partial t} = ADV\_W + PRESS\_W + BUOY\_W + DIFF\_W \tag{11}$$

While BUOY_W and PRESS_W represent different processes, these terms are often large and in opposition to each other. When BUOY_W and PRESS_W are in balance, and the other terms of

equation 2 are equal to zero, the atmosphere is in hydrostatic balance. Thus, examining BUOY_W+PRESS_W makes the overall thermodynamic effect on vertical velocity clearer than examining these terms individually.

The horizontal advection of the water vapor mixing ratio perturbation (ADV_H_rvp), vertical advection of water vapor mixing ratio perturbation (ADV_V_rvp), and diffusion of water vapor mixing ratio perturbation (DIFF_rvp) are defined as follows:

$$ADV\_H\_rvp = -\frac{\partial u r_v'}{\partial x} \tag{12}$$

$$ADV\_V\_rvp = -\frac{1}{\bar{\rho}}\frac{\partial \bar{\rho} w r_v'}{\partial z} - w\frac{d\overline{r_v}}{dz} \tag{13}$$

$$DIFF\_rvp = K_{hx}\frac{\partial^2 r_v'}{\partial x^2} + K_{hz}\frac{\partial^2 r_v'}{\partial z^2} \tag{14}$$

Thus equation 5 can be rewritten as follows.

$$\frac{\partial r_v'}{\partial t} = ADV\_H\_rvp\ + ADV\_V\_rvp + DIFF\_rvp \tag{15}$$

At initialization, $w = 0$ and $r_v' = 0$ throughout the domain, thus equation 2 can be simplified to the following.

$$\frac{\partial w}{\partial t} = -c_{p_d}\overline{\theta_v}\frac{\partial \pi'}{\partial z} + g\left(\frac{\theta'}{\bar{\theta}} + 0.61 r_v'\right) = \ PRESS\_W + BUOY\_W \tag{16}$$

Similarly, equation 5 can be simplified as the following.

$$\frac{\partial r_v'}{\partial t} = -w\frac{d\overline{r_v}}{dz} = \ ADV\_V\_rvp \tag{17}$$

Thus, the only processes that can produce vertical velocity from an initial absence of vertical velocity are buoyancy and a vertical perturbation pressure gradient, and the only process which can produce water vapor perturbations from an absence of water vapor is vertical advection, specifically vertical advection of base state water vapor. The remaining terms in equations 11

and 15 cannot be said to explicitly produce vertical velocity or water vapor perturbations, but rather simply move them around.

3.1 Processes Before a Cold Pool Collision

The processes associated with the temporal evolution of a cold pool collision are shown in Figures 3.1 through 3.5. Note that Figures 3.1-3.3 track the cold pool starting on the left side of the domain. They follow this cold pool as it propagates outwards to meet the cold pool on the right side of the domain. The latter figure panels show both cold pools participating in the collision. After 1 minute of simulation, the cold pool on the left side of the domain has changed little in shape from the initial temperature perturbation in the model (Figure 3.1a). At this time, subsident motion is present in the center of the cold pool leading to divergent flow at the surface. The cold pool is colder than the base state environment, leading to BUOY_W < 0 inside the cold pool (not shown); however, the negative temperature perturbation of the cold pool also leads to a positive pressure perturbation inside of the cold pool (Figure 3.2a). This positive pressure perturbation near the surface leads to PRESS_W > 0 (not shown). Thus, near the center of the cold pool, as |BUOY_W| > |PRESS_W|, subsident motion occurs due to the air being negatively buoyant. Conversely, near the edge of the cold pool, as |PRESS_W| > |BUOY_W|, air is accelerated upwards due to a positive vertical perturbation pressure gradient force (Figure 3.2a). At 1 minute, a small decrease in water vapor mixing ratio also exists in the center of the cold pool (Figure 3.3a) as a result of the subsident motion inside of the cold pool that advects dry air from above downwards into the cold pool leading to ADV_V_rvp < 0 (Figure 3.3a).

After 6 minutes the cold pool has rapidly flattened to a maximum height of ~500 m and spread ~1.5 km towards the center of the domain (Figure 3.1b). As this cold pool advances

towards the center of the domain, typical cold pool behavior is evident, with rising motion at the cold pool head, and subsident motion behind it (Goff 1976) (Figure 3.1b-d). As at 1 minute, rising motion is driven by a positive vertical perturbation pressure gradient force in front of the cold pool head and subsident motion behind the cold pool head by negative buoyancy in this region (Figure 3.2b-d). Density potential temperature increases within the cold pool from 6 minutes to 18 minutes, thereby reducing the perturbation from the environment and weakening the cold pool (Figure 3.1b-d). As there is no source of diabatic heating or cooling following the initialization of the simulations, this progressive dissipation is due to the entrainment of environmental air into the cold pool. This entrainment weakens the lifting at the cold pool edge and the subsidence behind the cold pool head. Both the buoyant force and vertical perturbation pressure gradient force are reduced in magnitude as a result, leading to an overall reduction in magnitude of BUOY_W+PRESS_W (Figure 3.2b-d). The rising motion and associated vertical advection of water vapor at the cold pool edge (Figure 3.3b-d) results in moistening at the cold pool edge up through 18 minutes (Figure 3.1c-d).

3.2 Processes During a Cold Pool Collision

The two cold pools collide at the center of the domain at 24 minutes (Figure 3.1e and Figure 3.4); this is also the time period in which the largest domain maximum vertical velocity is observed. The pressure is locally enhanced at the surface at the location of the collision (Figure 3.2e), as a result of the large horizontal convergence associated with the collision (Eq. 4). This produces a large, positive PRESS_W+BUOY_W below ~400 m at the location of the collision, thereby accelerating air upwards. Collocated with this positive PRESS_W+BUOY_W are negative values of vertical velocity advection. Above ~400 m, the signs of these two trends

reverse, with PRESS_W+BUOY_W < 0 and ADV_W > 0 (Figure 3.2e). This change in sign in the vertical velocity advection is indicative that the vertical velocity produced below 400 m is being transported to above 400 m. Above 400 m, PRESS_W+BUOY_W < 0 as the air lofted during the collision is negatively buoyant as a result of two processes. Firstly, some of the air lofted by the collision originates within the cold pools and hence is negatively buoyant. Secondly, the WK environment is stably stratified and thus, as air rises, its perturbation potential temperature decreases.

The collision-induced increase in vertical velocity increases the water vapor mixing ratio (Figure 3.3e) and occurs in a similar matter to the vertical velocity. Below 400 m, large horizontal advection increases the water vapor content at the location of the collision, while vertical advection lifts it (Figure 3.3e). Above 400m, vertical advection increases moistening at the location of the collision while the horizontally divergent flow decreases the water vapor content.

3.3 Processes After a Cold Pool Collision

As time progresses after the collision, the aforementioned negative buoyancy deaccelerates the updraft. Six minutes after the collision, at the location of the collision, the air weakly subsides due to this negative buoyancy, while the water vapor remains enhanced (Figure 3.1f). This negative buoyancy, however, is nearly balanced by a positive vertical perturbation pressure gradient force leading to minimal positive or negative acceleration of the updraft, as the atmosphere is nearly in hydrostatic balance (Figure 3.2f). The weakly subsiding motion decreases the water vapor mixing ratio at 30 minutes, but at rates much slower than the moistening during the collision (Figure 3.3f).

3.4 Figures

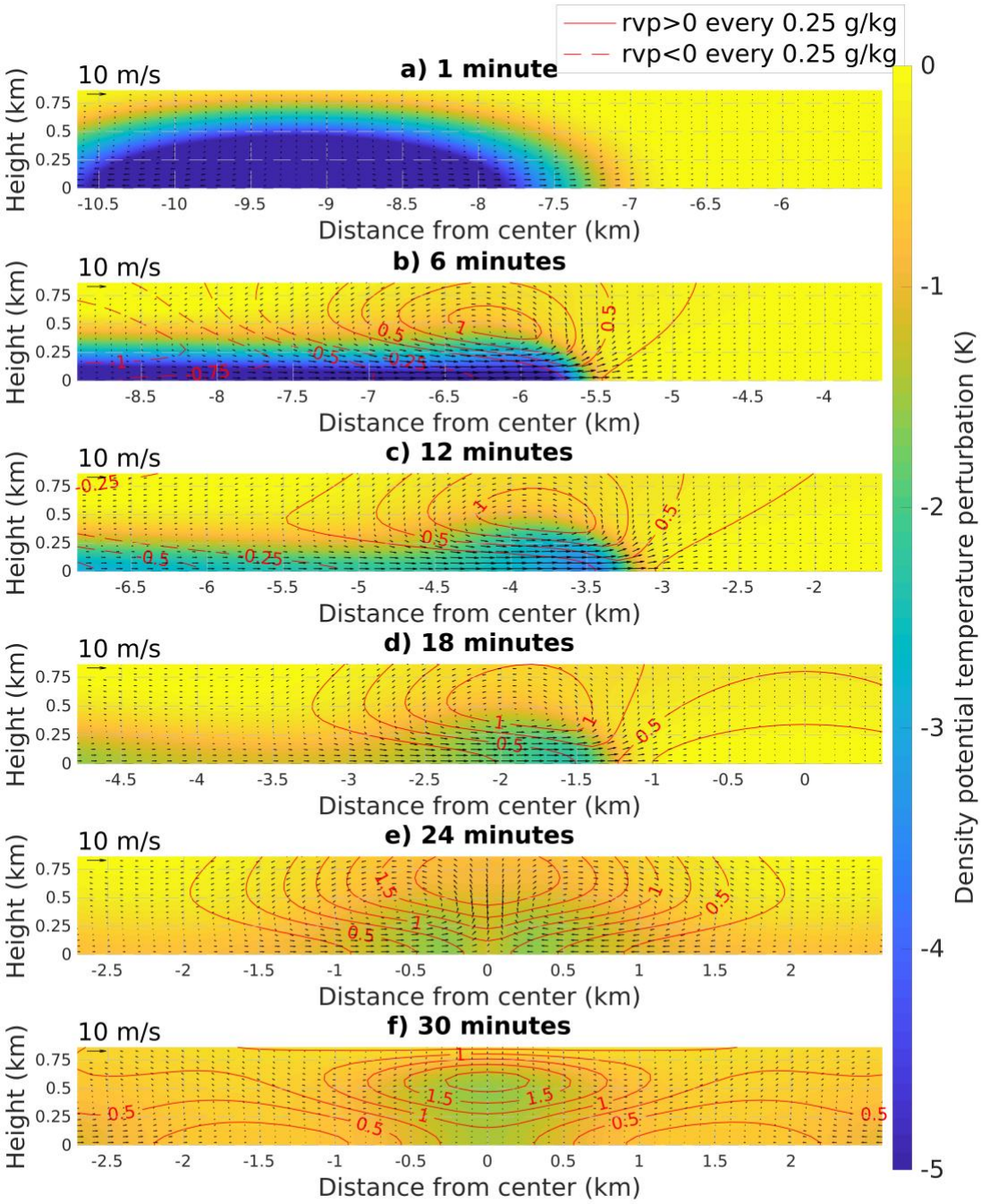

Figure 3.1: The evolution of colliding cold pools over the first 30 minutes of the simulation. Density potential temperature perturbation (shaded), water vapor mixing ratio perturbation (red contours every 0.25 g kg^{-1}), and winds for the WK_T10_D136 simulation at (a) 1,(b) 6, (c) 12,

(d) 18, (e) 24, and (f) 30 minutes are shown. Note that the portion of the domain shown is focused on the cold pool on the left side of the domain, and that is moves in time as the cold pool propagates. The symmetric initialization of the model domain means that the cold pool on the right side of the domain is a mirror image of the left cold pool. The right cold pool does become evident in panel (e). This figure is plotted so that the aspect ratio of the cold pool is generally preserved.

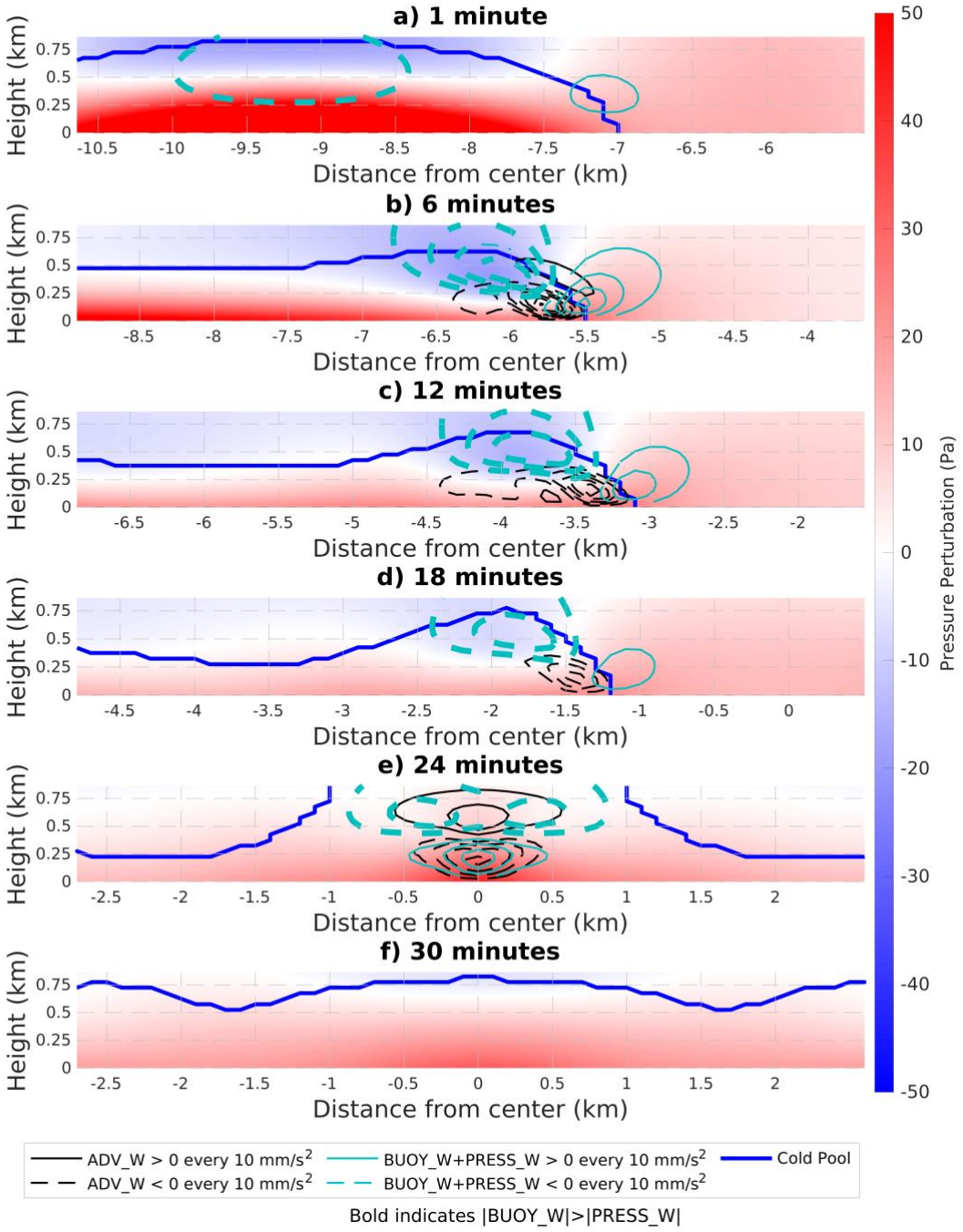

Figure 3.2: Dynamics of two colliding cold pools over the first 30 minutes of the simulation. As in Figure 3.1 but showing perturbation pressure (shaded), advection of vertical velocity (ADV_W see equation 7) (black contours), the sum of the buoyancy term and vertical perturbation pressure gradient term (BUOY_W+PRESS_W see equations 8 and 9) (sky-blue contours), and the cold pool boundary (dark blue line) for the WK_T10_D136 simulation at (a) 1,(b) 6, (c) 12, (d) 18, (e) 24, and (f) 30 minutes. Thick sky-blue contours indicate the magnitude of BUOY_W is greater than that of PRESS_W. Thin sky-blue contours indicate the magnitude of

PRESS_W is greater than that of BUOY_W. All contours every 10 mm s^{-2}. Diffusion of vertical velocity (DIFF_W) not plotted due to being much weaker than ADV_W and BUOY_W+PRESS_W.

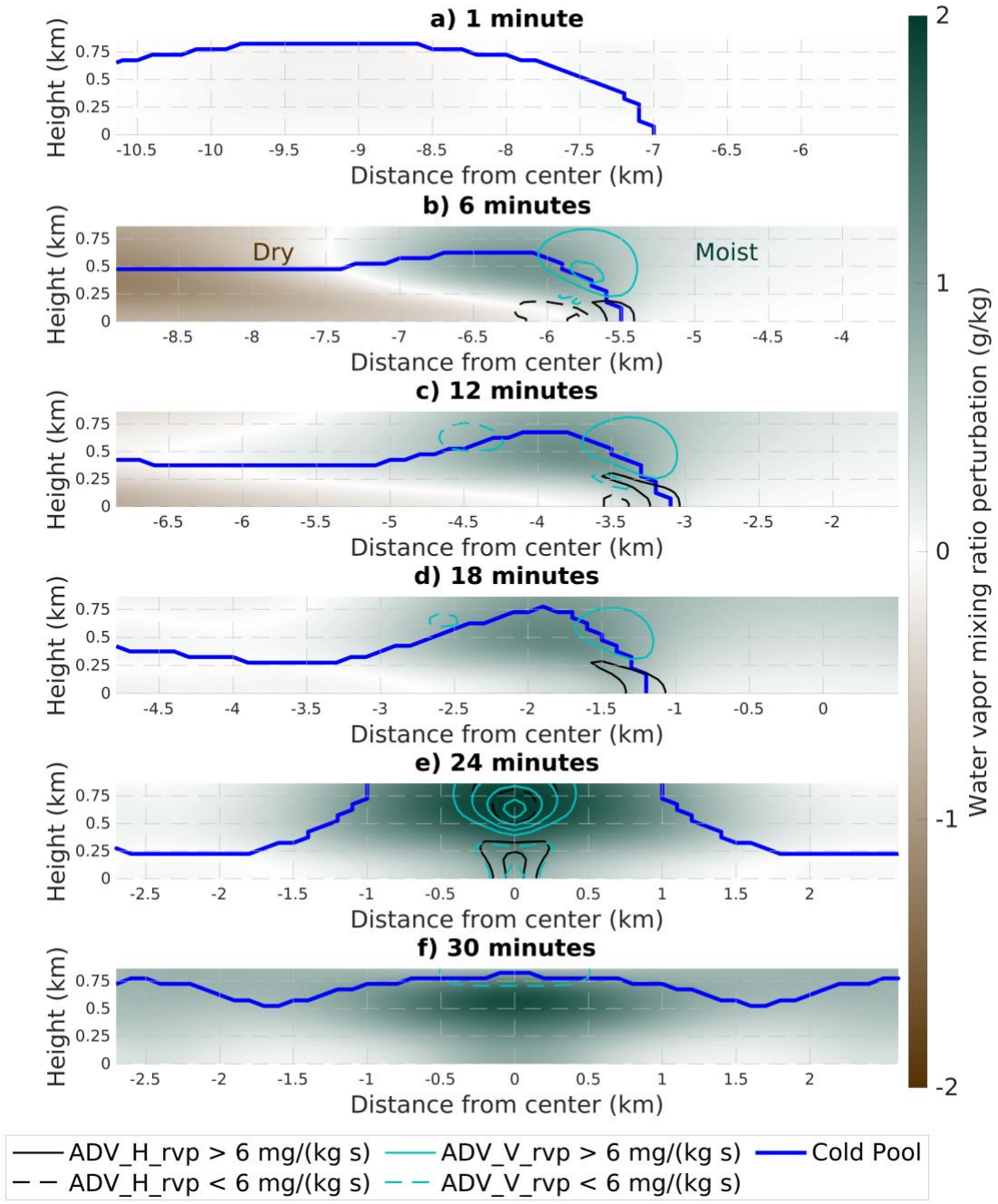

Figure 3.3: Moisture transport associated with colliding cold pols over the first 30 minutes of the simulation. As in Figure 3.1 but showing water vapor mixing ratio perturbation (shaded), horizontal advection of water vapor mixing ratio perturbation (ADV_H_rvp; equation 12) (black contours), vertical advection of water vapor mixing ratio perturbation (ADV_V_rvp; equation 13) (sky-blue contours), and the cold pool boundary (dark blue line) for the WK_T10_D136 simulation at (a) 1, (b) 6, (c) 12, (d) 18, (e) 24, and (f) 30 minutes. All contours are at every 6 mg

kg^{-1} s^{-1}. Diffusion of water vapor mixing ratio perturbation (DIFF_rvp) is not plotted due to being much weaker than ADV_H_rvp and ADV_V_rvp.

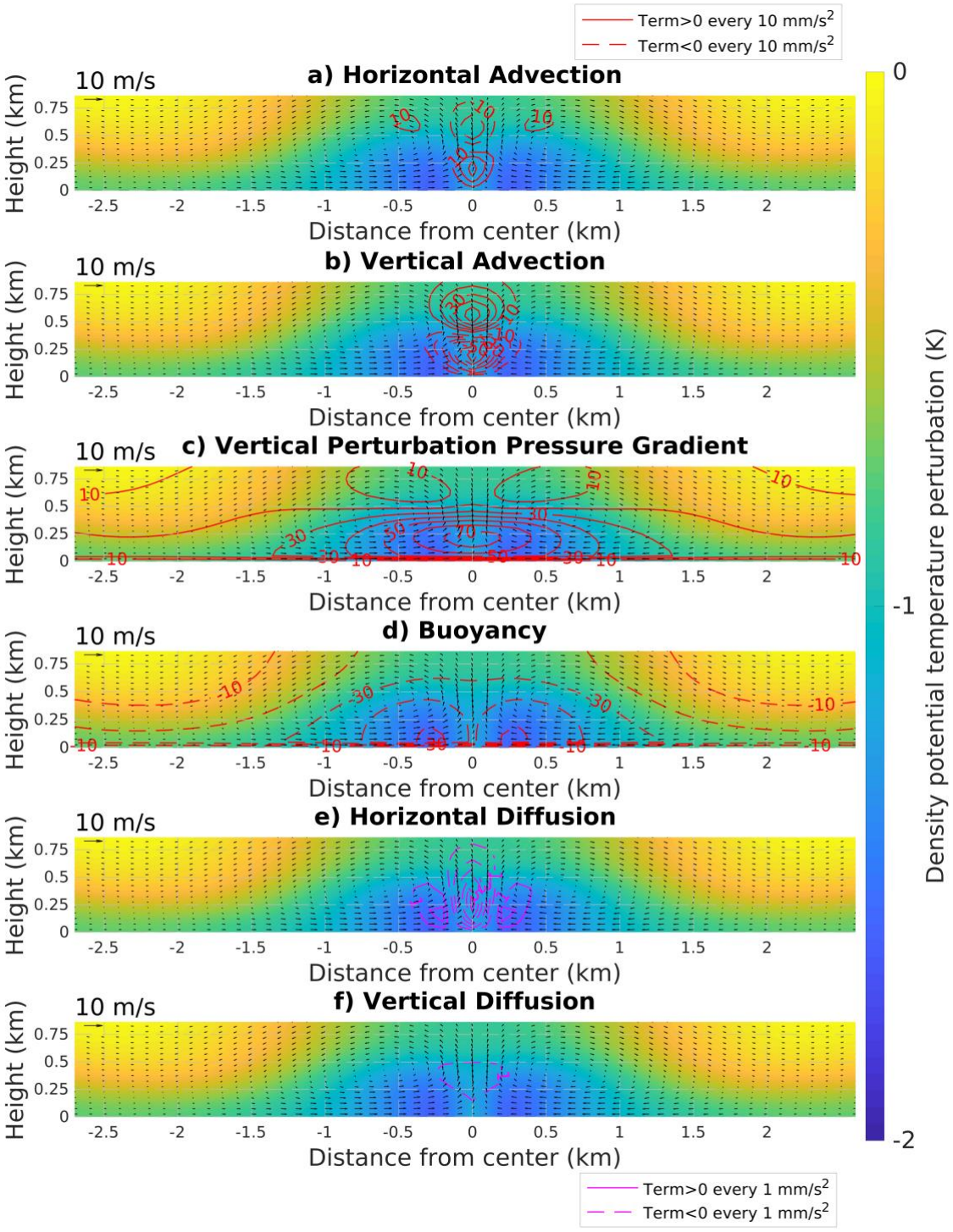

Figure 3.4: Terms of the vertical velocity tendency equation (Eq. 2) during a cold pool collision occurring at 24 minutes into the simulation. Density potential temperature perturbation (shaded) and winds for the WK_T10_D136 simulation are shown in all panels. Contours of (a) horizontal advection of vertical velocity, (b) vertical advection of vertical velocity (red), (c) the vertical perturbation pressure gradient term of the vertical velocity equation, and (d) buoyancy every 10

mm s^{-2} in red. Contours of (e) horizontal diffusion and (f) vertical diffusion are shown at every 1 mm s^{-2} in magenta.

Chapter 4: Exploring the Parameter Space of Cold Pool Collisions

In this chapter, the effects of the initial cold pool temperature perturbation, initial distance between cold pools, strength of the diffusion, and the thermodynamic environment on cold pool collisions are now addressed. The relative importance of each parameter is then assessed. Much of this analysis utilizes the domain and time maximum vertical velocity (hereafter W_max) and water vapor mixing ratio perturbation (hereafter rvp_max) from the simulations. Given that cold pool collisions generate new convection by locally increasing vertical velocity and water vapor content in the region of the collision, W_max is used as a proxy for mechanical forcing and rvp_max is used as a proxy for thermodynamic forcing. Throughout this analysis, it is also often helpful to think in terms of kinetic and potential energy. An initially motionless cold pool has no kinetic energy but achieves a maximum in gravitational potential energy as a result of the presence of dense fluid above the surface. As the cold pool spreads out horizontally, the potential energy is converted to kinetic energy. Cold pools with larger initial temperature perturbations are referred to as “more intense” while cold pools with smaller initial temperature perturbations are referred to as “less intense”.

4.1 The Effect of the Initial Temperature Perturbation

The WK experiment suite demonstrates that as the initial cold pools become more intense, collisions between these cold pools generate monotonically increasing W_max and rvp_max (Figure 4.1). This is also true in the mean for all of the other environments considered (Figure 4.2a,c). Consequently, more intense initial cold pools have a greater chance to initiate new convection. Furthermore, a cold pool that was initially more intense will remain colder, and

hence more intense, than a cold pool that was initially less intense (Figure 4.3a). Thus, a pair of initially more cold pools will be colder when they collide than will a pair of initially warmer, weaker cold pools. Colder cold pools also have greater horizontal winds at their outflow boundaries (Figure 4.3a,c). This relationship arises from the fact that colder cold pools have more potential energy to convert to kinetic energy. More intense initial cold pools will therefore produce greater horizontal convergence, thereby leading to a greater near-surface pressure perturbation at the point of the collision, which in turn drives stronger updrafts. The stronger updrafts enhance the vertical advection of water vapor, thereby moistening the atmosphere during the collision.

4.2 The Effect of the Initial Distance

The relationship between the initial cold pool distance and W_max in the WK experiment suite is non-monotonic (Figure 4.1a). W_max peaks around an "optimal distance" of ~2.5 km and decreases for distances smaller or larger than this optimum. Peak W_max at this ~2.5 km optimal distance is evident across the other experiment suites as well (Figure 4.2b). The relationship between rvp_max and initial distance is also nonmonotonic in the WK experiment suite (Figure 4.1b). Unlike with W_max, peak values of rvp_max occur for much greater optimal distances than W_max, especially as the intensity of the initial cold pools increases (Figure 4.1b). The peak rvp_max can be explained when we consider the role of vertical advection. Under strong vertical advection, water vapor is rapidly vertically advected as well as laterally transported. Under weak vertical advection, both the vertical and lateral transport are weak. Thus, large updrafts do not always imply large enhancements in water vapor mixing ratio. As a result, W_max and rvp_max have different relationships with the initial cold pool distances.

Time series of the domain maximum vertical velocity for the 10 K simulations of the WK, DI, NT, and SK experiment suites are shown in Figure 4.4a-d in the purple to yellow lines. The red and black lines will be explained later. The peaks of these curves correspond with the cold pool collisions. It is clear from this figure that as the initial separation distance increases (indicated by lighter colored lines), the collisions occur later and later in time. This behavior is expected and was also seen in MH20's figure 7a. The optimal distance is also evident in this figure, as in each subplot, the highest peak is not for the most closely spaced cold pools (the darkest of purple lines) but rather for those starting out slightly further apart (lighter purple lines). Enhancements in water vapor due to cold pool collisions decrease more slowly and, in some cases, nonmonotonically with time than those for vertical velocity (Figure 4.4e-h). Additionally, comparing the timing of these enhancements in the WK suite demonstrates that peaks in water vapor mixing ratio occur after those in vertical velocity for all of the experiments (Figure 4.4i). This can be explained by the fact that the water vapor mixing ratio perturbations are generated by the collisional updraft, so they only decrease once that updraft has collapsed.

Cold pools which start closer together will be colder when colliding, so as the initial distance between cold pools decreases, W_max should increase. This is the case for all but the closest initial distances tested, where this trend reverses. This reversal can be explained in terms of kinetic and potential energy.

The domain-integrated kinetic energy from simulations in the WK experiment suite is shown in Figure 4.5. The increase in kinetic energy in this figure is due to the fact that it takes time for the cold pools to generate kinetic energy from their initial potential energy, while the decrease in kinetic energy is due to the dissipation of the cold pools. A balance between the generation of kinetic energy and dissipation of the cold pools explains the optimal distance. For

cold pools which start closer together than the optimal distance of ~2.5km, the cold pools do not have sufficient time to convert sufficient potential energy into kinetic energy before colliding, resulting in reduced convergence during the collision, and thus diminished W_max. For cold pools which start further apart than the optimal distance, the cold pools have dissipated appreciably before colliding, thereby reducing kinetic energy and resulting in diminished W_max.

The different phases of density current evolution (Huppert and Simpson 1980) could also serve as an explanation for the optimal distance. It seems logical that cold pools which are too close together and collide during the initial acceleration or the slumping phase would have diminished W_max due to motions in the surrounding atmosphere slowing cold pool propagation. However, such motions would be insignificant to cold pools which collide during the inertial phase. Thus, a pair of cold pools spaced so that they collide early in the inertial phase, before they have slowed appreciably, would seemingly have the greatest W_max. This line of reasoning is speculative, and further analysis is needed to confirm this explanation of the optimal distance in terms of density current phases. Note that the cold pools in these simulations will not enter a viscous phase, as the model used is inviscid.

With the relationship between the W_max and the initial distance between cold pools now explained, Figure 4.4a can also be used to define “strong” and “weak” collisions. It should first be noted that all of the cold pools in these simulations produce rising motion at their leading edges, even when collisions are not occurring. At each timestep, the red “minimum line” drawn in Figure 4.4a represents the minimum domain maximum vertical velocity from all of the WK, DI, NT and SK experiments (purple to yellow lines). It is notable that for any given simulation, the domain maximum vertical velocity from that simulation closely tracks the red minimum line

with the exception of when the cold pool collision is occurring in the given simulation. During the collision, the domain maximum vertical velocity in that simulation peaks above the red minimum line. Thus, the red minimum line represents the vertical velocity produced by otherwise identical cold pools which do not collide, as the effect of collision is removed. A black horizontal line is plotted at 1.1 times the peak of this red minimum line, thus indicating the W_max that would be produced from a pair of non-colliding cold pools acting on their own. In the WK environment (Figure 4.4a), for initial distances of 16.8 km and greater (green to yellow lines), the peak vertical velocities produced from the cold pool collisions are less than this black horizontal line. This means that the vertical velocity produced by collisions of cold pools starting at these initial distances apart is less or not substantially greater than the W_max produced from the individual cold pools acting on their own. A distinction can be made between collisions which produce substantially greater W_max than the individual cold pool action, hereafter called "mechanically strong", and collisions whose peak vertical velocity is less than the W_max from individual cold pool action, hereafter called "mechanically weak". A black vertical line is included in figure 4.4a to separate the last mechanically strong collision from the first mechanically weak collision.

Similar red and black lines are plotted in Figure 4.4b-d to identify mechanically strong and weak collisions from the simulations plotted; note that the DI environment in figure 4.4b has no mechanically weak collisions. "Thermodynamically strong" and "thermodynamically weak" collisions are defined using the same method described above for mechanically strong/weak collisions, except timeseries of domain maximum water vapor mixing ratio perturbation are used instead of timeseries of domain maximum vertical velocity (Figure 4.4e-h).

By definition, the mechanically strong collisions indicated in Figure 4.4a-d produce greater W_max than the actions of individual cold pools, but the mechanically weak collisions do not. Hence, in this framework, mechanically strong cold pool collisions increase the probability of convective initiation beyond that of the individual action of the pre-collision cold pools. Mechanically weak collisions, on the other hand, do not increase the odds of convective initiation beyond the action of the individual cold pools. This terminology of mechanically strong and weak collisions is therefore proposed as a simple binary metric to determine if a collision meaningfully increases the probability of convective initiation, in the absence of thermodynamic forcing. By analogous logic, in the absence of mechanical forcing, thermodynamically strong cold pool collisions increase the probability of convection initiation beyond that of the individual action of the pre-collision cold pools while thermodynamically weak collisions do not.

4.3 The Effect of Diffusion Strength

Decreased diffusion reduces the rate at which cold pools dissipate (Figure 4.3b) which leads to increased horizontal wind throughout the lifetime of the cold pools (Figure 4.3d) and hence greater W_max and rvp_max. Cold pool collisions with decreased diffusion (suites labeled "HK") have greater W_max, greater rvp_max, and more mechanically and thermodynamically strong collisions than collisions with standard diffusion, irrespective of variations in cold pool strength and the distance between them (Figure 4.2). These trends are reversed for simulations with increased diffusion (suites labeled "DK"). Hence, decreased diffusion enhances the chance of convective initiation.

4.4 The Effect of the Environment

Two specific environmental factors form the focus of the environmental effects on cold pool collisions. The first is the low-level static stability, defined as the base state Brunt-Väisälä frequency between 25 m to 975 m AGL. The second is the low-level differential moisture, defined here as the base state water vapor mixing ratio at 25 m AGL minus the base state water vapor mixing ratio at 975 m AGL. These levels are chosen as 25 m AGL is the lowest scalar model level while 975 m AGL is the highest scalar model level below 1000 m AGL, which is the top of the initial cold bubbles.

Comparing the DI, NT_HS, NT, and NT_DS experiment suites, where the low-level static stability steadily increases from 0 to 0.02 s^{-1}, it is clear that increasing the low-level static stability decreases the W_max produced by collisions and the percentage of mechanically strong collisions (Figure 4.2a,b,e,f). This is due to both the stabilization effect, in which there is greater resistance to upward motion as low-level static stability is increased, and seemingly also the effect of gravity waves. Liu and Moncrieff (2000) argued that radiation of energy by gravity waves does not apply to cases in which low-level stable layers trap gravity waves within the layer. However, domain total kinetic energy in experiments with any static stability, whether limited to the surface (NT, NT_HS, NT_DS, and gray lines), or in a continuously stratified atmosphere (SK_HK and gray lines), is significantly reduced compared to the experiments using a dry isentropic environment (DI, DI_HK, DI_DK) (Figure 4.6). Thus, it appears that while gravity waves remain trapped near the surface in the nocturnal cases (NT, NT_HS, NT_DS, NT_HK, and NT_DK), they are still capable of radiating energy away from the cold pools and dissipating it as in the continuously stratified atmospheres. However, it is unclear how to

disentangle the stabilization effect from the effect of gravity waves, as both will occur in statically stable environments, and to compare their individual impacts on W_max.

The effect of even minimal low-level static stability on cold pool collisions can be significant. The dry isentropic (DI, DI_HK, DI_DK) and half-stability nocturnal (NT_HS) experiment suites were rerun for 4 hours to examine this effect. These suites were chosen as DI, DI_HK, and DI_DK have no low-level static stability, while NT_HS has the lowest non-zero value of any of the environments tested, with low-level static stability of 0.005 s^{-1}. For large initial cold pool distances and the least intense initial temperature perturbations, collisions may not occur within the 1-hour time simulation duration. Rerunning NT_HS for four hours (Figure 4.7d) demonstrates that even with minimal low-level static stability, collisions cease to be mechanically strong well before an hour of simulation time, as the cold pools with a 1 K initial perturbation dissipate quickly. However, this is not the case in DI, DI_HK, or DI_DK suites, where all of the collisions are mechanically strong, even with the least intense initial temperature perturbation (1 K) and furthest initial distance (27.2 km) tested (Figure 4.7a-c).

Finally, comparing the WK, S10, SK, and S07 simulations, with low-level differential moisture of 3.2, 4.5, 6.5, and 7.2 g kg^{-1} respectively, it is clear that as differential moisture increases, rvp_max increases (Figure 4.2c,d). This is due to the vertical advection of base state water vapor (Eq 5). For the same positive vertical velocity, a greater differential moisture will lead to a greater positive increase in water vapor mixing ratio perturbation with time.

4.5 Relative Importance and Summary of Effects

The differences in W_max between the maximum and minimum values for all of experiment suites and for all of the parameters tested here are shown in Figure 4.8a. This

indicates that the chance for convective initiation is most sensitive to the initial temperature perturbation, followed by the low-level static stability, initial cold pool distance, and lastly the diffusion strength (Figure 4.8a). The chance for convective initiation increases nearly linearly as cold pools get colder (Figure 4.8b), peaks at the optimal distance of ~2.5 km and decreases away from that distance (Figure 4.8c), decreases slightly with increased diffusion (Figure 4.8d), and nonmonotonically decreases as low-level static stability increases (Figure 4.8e).

Similarly, the impact of each parameter on rvp_max is summarized in Figure 4.9. Convective initiation via thermodynamic forcing is most sensitive to the initial temperature perturbation, followed by the low-level differential moisture, initial cold pool distance, and finally the diffusion strength (Figure 4.9a). Thermodynamic forcing greatly increases as cold pools get colder (Figure 4.9b), slowly and nonmonotonically decreases as initial distance increases (Figure 4.9c), decreases slightly with enhanced diffusion (Figure 4.9d), and greatly increases as low-level differential moisture strengthens (Figure 4.9e).

It is important to note that for both vertical velocity and water vapor, the predominance of the tested parameters is the same. *The chance of convective initiation is therefore greatest for colliding cold pools which start as cold as possible, at the optimal distance, with minimal diffusion, and in an environment with low static stability and a large vertical gradient in water vapor.*

4.6 Figures

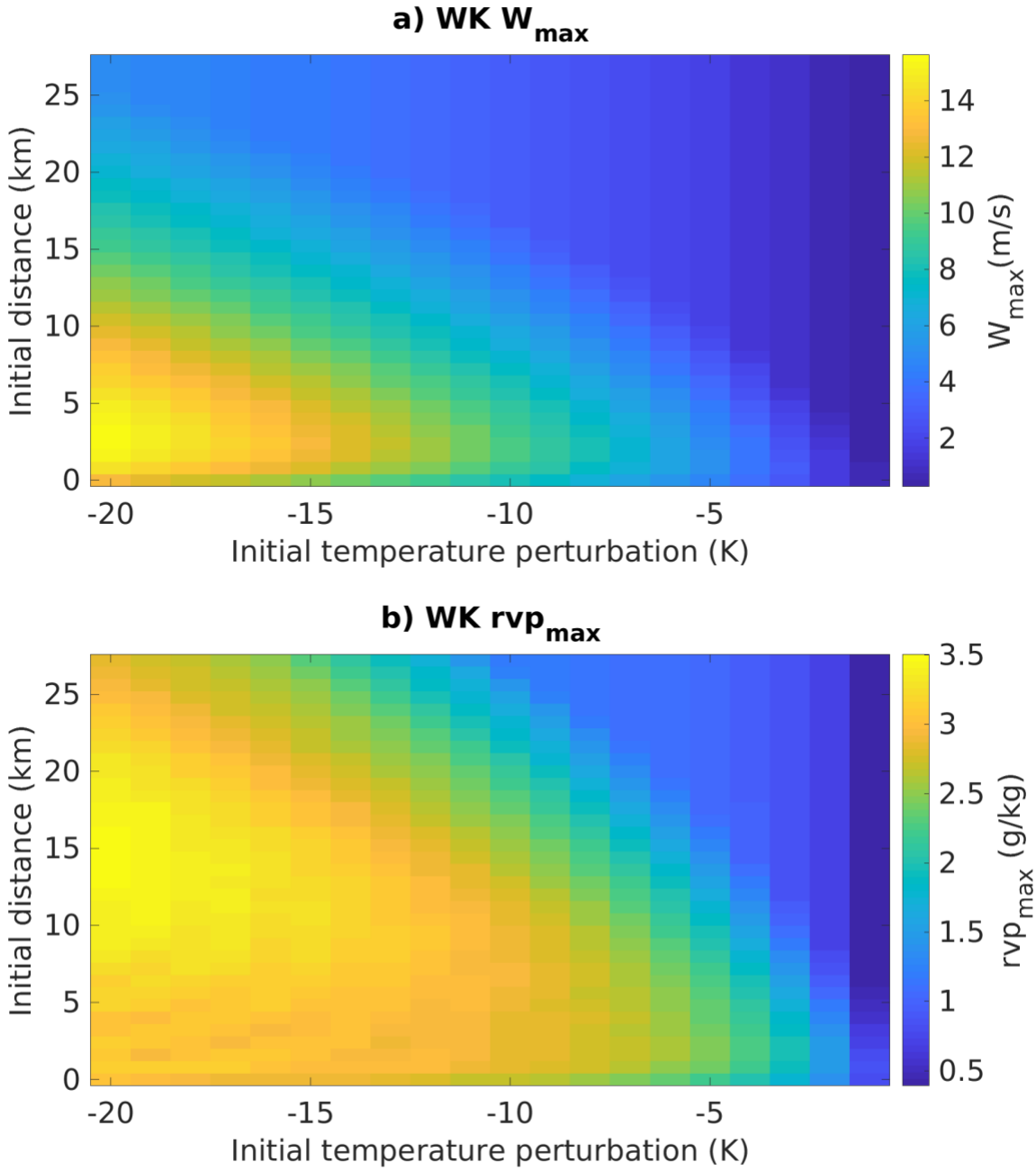

Figure 4.1: Change in the proxies of mechanical and thermodynamic forcing from cold pool collisions with initial distance and initial temperature perturbation. (a) W_max and (b) rvp_max from all simulations in the WK experiment suite. Note the "0" initial distance row indicates simulations in which the initial cold pools start with their edges touching.

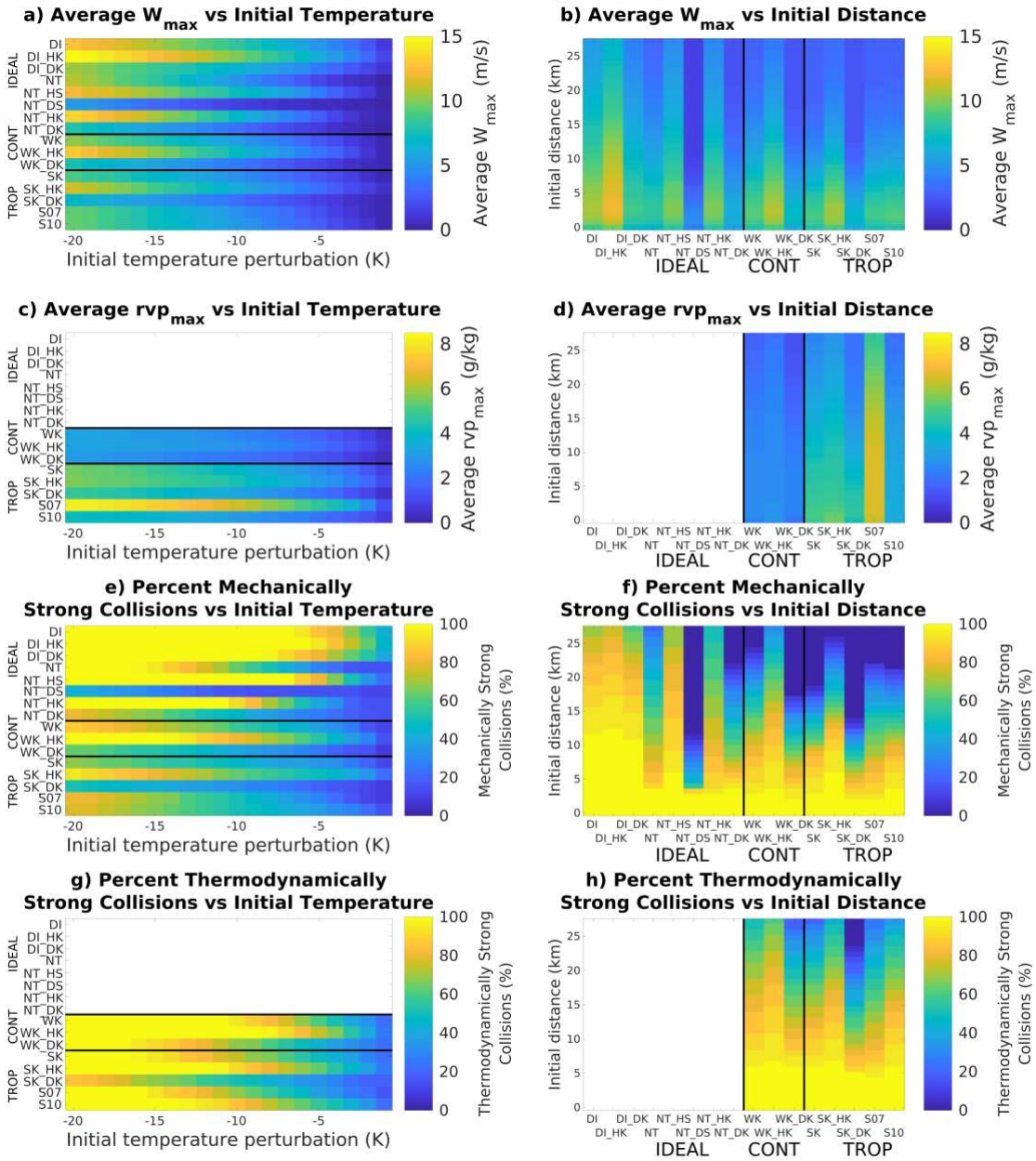

Figure 4.2: Summary of mechanical forcing and thermodynamic forcing from all the experiment suites. The (a, b) W_max, (c, d) rvp_max, (e, f) percent of collisions that are mechanically strong (see chapter 4.2 for this definition), and (g, h) percent of collisions that are thermodynamically strong (see chapter 4.2 for this definition) for (left column) all experiments averaged over all initial distances, and (right column) all initial temperature perturbations. Note that no moisture is present in the IDEAL group of simulations, so the respective areas for these experimental suites is left blank in (c), (d), (g), and (h).

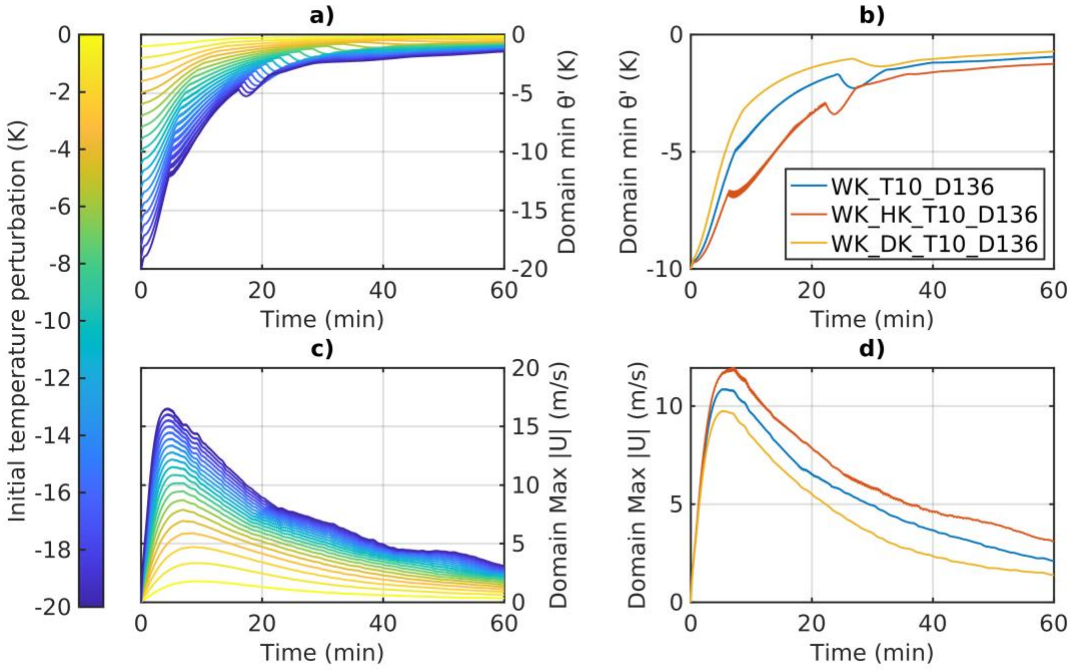

Figure 4.3: The effect of the initial temperature perturbation and diffusion strength on cold pool dissipation and horizontal winds. Timeseries of domain minimum potential temperature perturbation for (a) all simulations in the WK suite with an initial distance of 13.6 km and (b) the WK_T10_D136, WK_HK_T10_D136, and WK_DK_T10_D136 simulations. Timeseries of domain maximum absolute value of horizontal wind for (c) all simulations in the WK suite with an initial distance of 13.6 km and (d) the WK_T10_D136, WK_HK_T10_D136, and WK_DK_T10_D136 simulations. Darker colors in (a) and (c) indicate colder initial cold pool temperature perturbations as indicated by the legend.

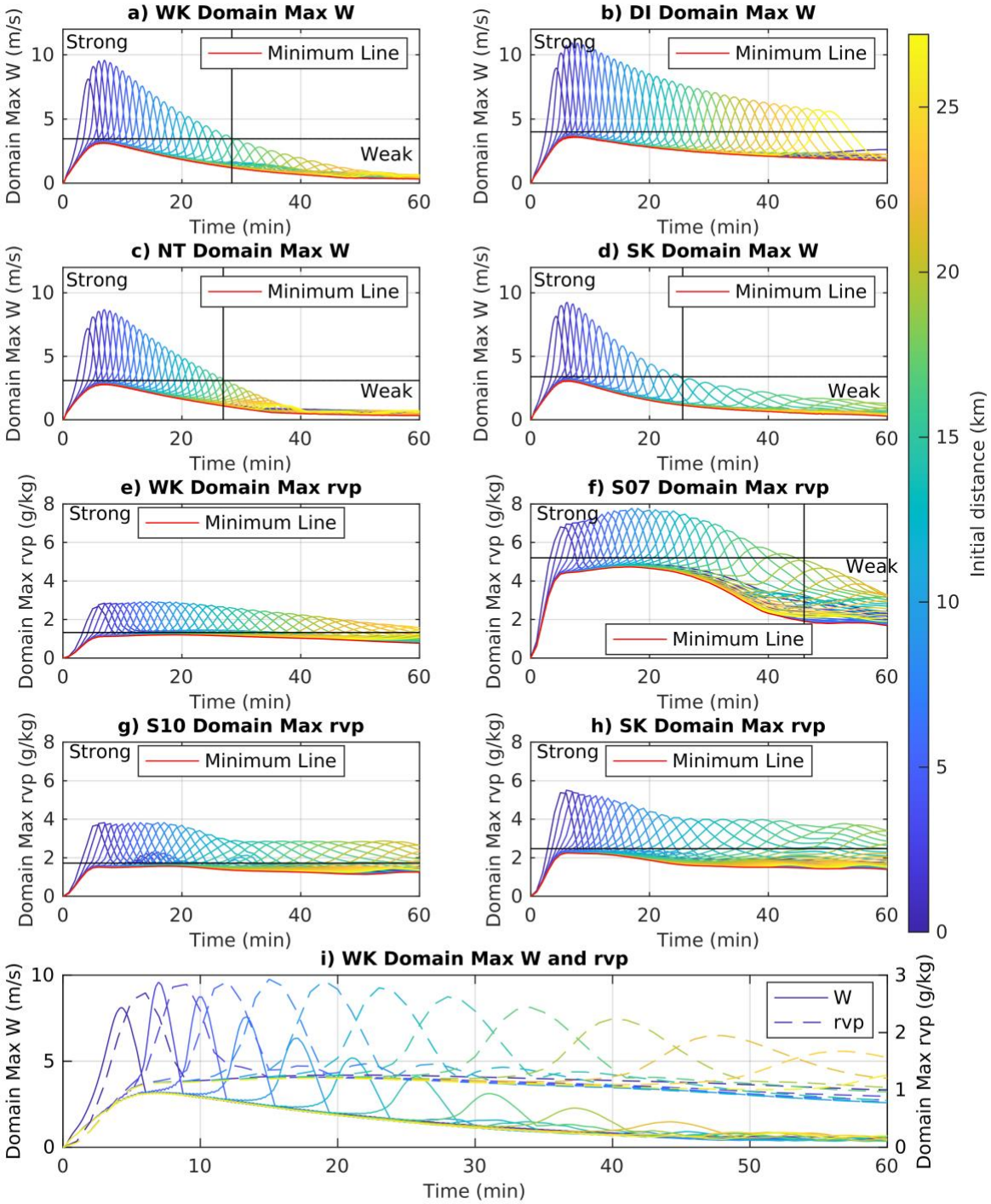

Figure 4.4: Timeseries of domain maximum vertical velocity from the 10 K initial minimum perturbation simulations from the (a) WK, (b) DI, (c) NT, and (d) SK experiment suites. Lighter colors indicate simulations with larger initial distances between cold pools. The red line is the

smallest domain maximum vertical velocity at each time, and the horizontal black line is 1.1 times the peak of this red line. Simulations with peaks above this horizontal black line have mechanically strong collisions (as defined in section 4.2). A vertical black line is placed to separate the last strong collision from the first weak collision. Those below and to the right of the black lines have weak collisions. All collisions in DI are strong. Timeseries of domain maximum water vapor mixing ratio perturbation from the 10 K initial minimum perturbation simulations from the (e) WK, (f) S07, (g) S10, and (h) SK experiment suites. Thermodynamically strong collisions indicated in (e-h) are analogous to mechanically strong collisions in (a-d). (i) Domain maximum vertical velocity (solid lines) and water vapor mixing ratio perturbation (dashed lines) are overlayed for 10 K initial minimum perturbation simulations and every third initial distance tested in the WK experiment suite.

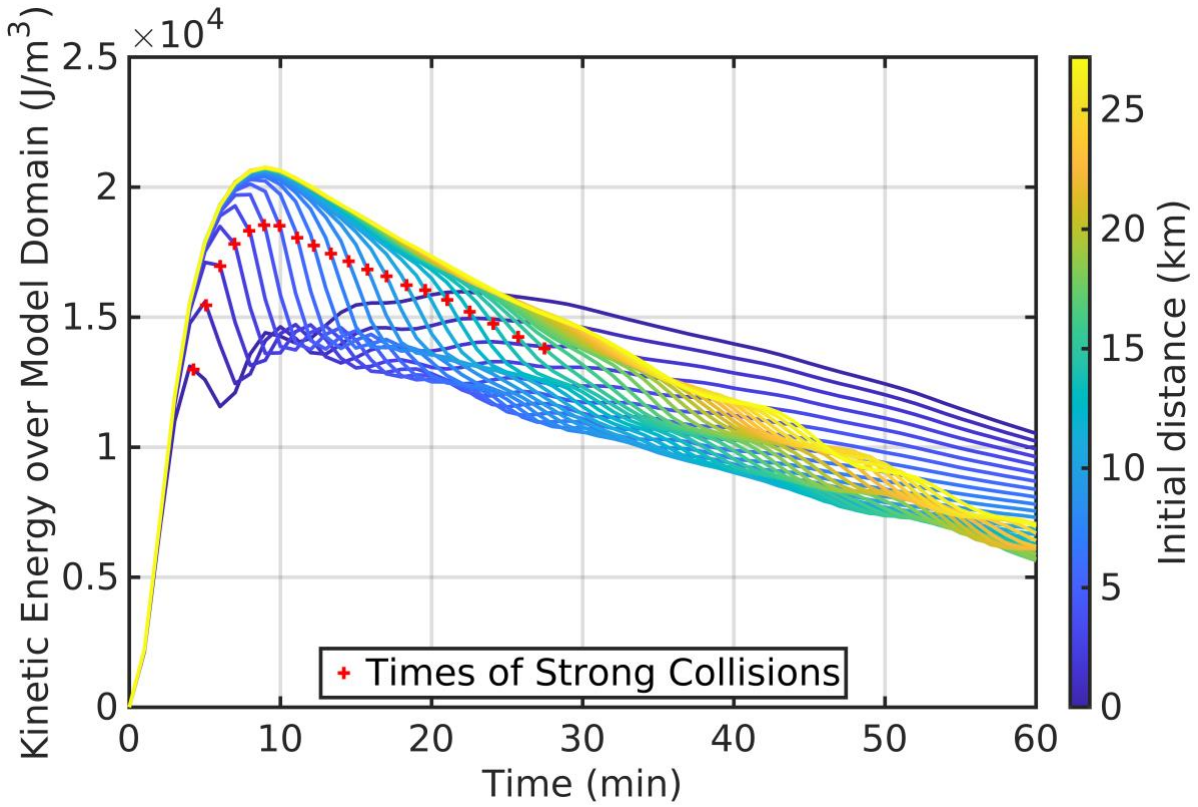

Figure 4.5: Evolution of the kinetic energy during cold pool collisions. Shown is the timeseries of kinetic energy summed over the model domain from the 10 K initial minimum perturbation simulations of the WK experiment suite. As in figure 4.4, lighter colors indicate simulations with larger initial distances between cold pools. For every simulation with a strong collision, a red cross (+) is placed that simulation's line marking the time the cold pools collide.

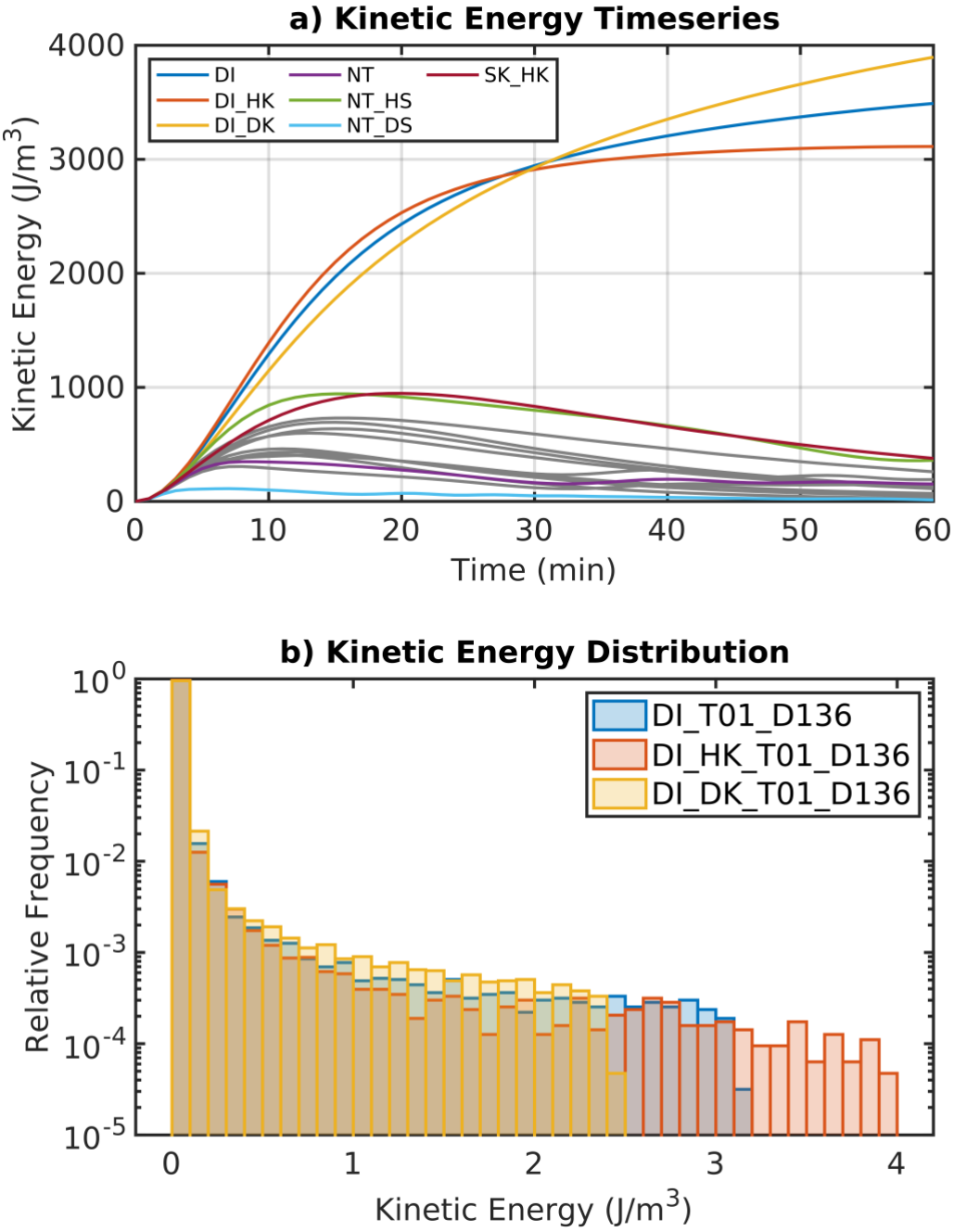

Figure 4.6: The effect of static stability on cold pool kinetic energy. (a) Timeseries of kinetic energy summed over the model domain for all simulations with an initial 1 K temperature perturbation and an initial distance of 13.6 km. Simulations not labeled with colored lines are plotted in gray for clarity and to demonstrate the difference between DI, DI_HK, and DI_DK and the rest of the environments. (b) Histogram of the spatial distribution of kinetic energy in the DI_T10_D136, DI_HK_T10_D136, and DI_DK_T10_D136 simulations after 60 minutes of simulation time.

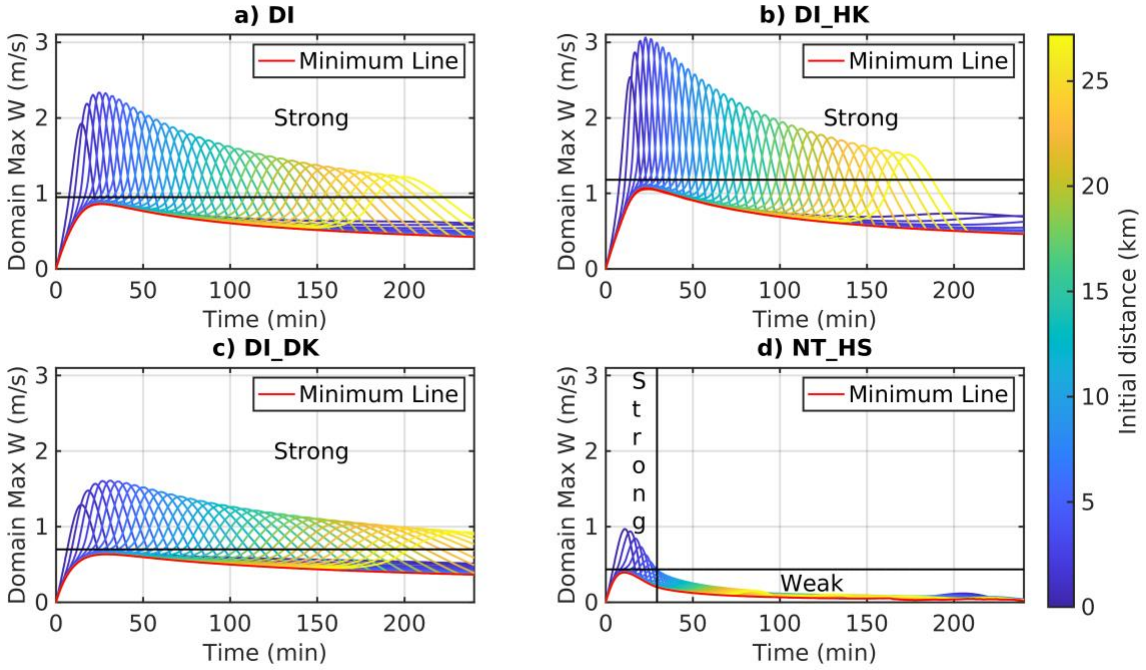

Figure 4.7: Effect of static stability on vertical velocity from cold pool collisions. As in Figure 4.4a-d, except for the 1 K initial minimum perturbation simulations from the (a) DI, (b) DI_HK, (c) DI_DK, and (d) NT_HS experiment suites after 4 hours. Note that all of the collisions are strong (see chapter 4.2 for definition) in the environments with no static stability (DI, DI_HK, and DI_DK).

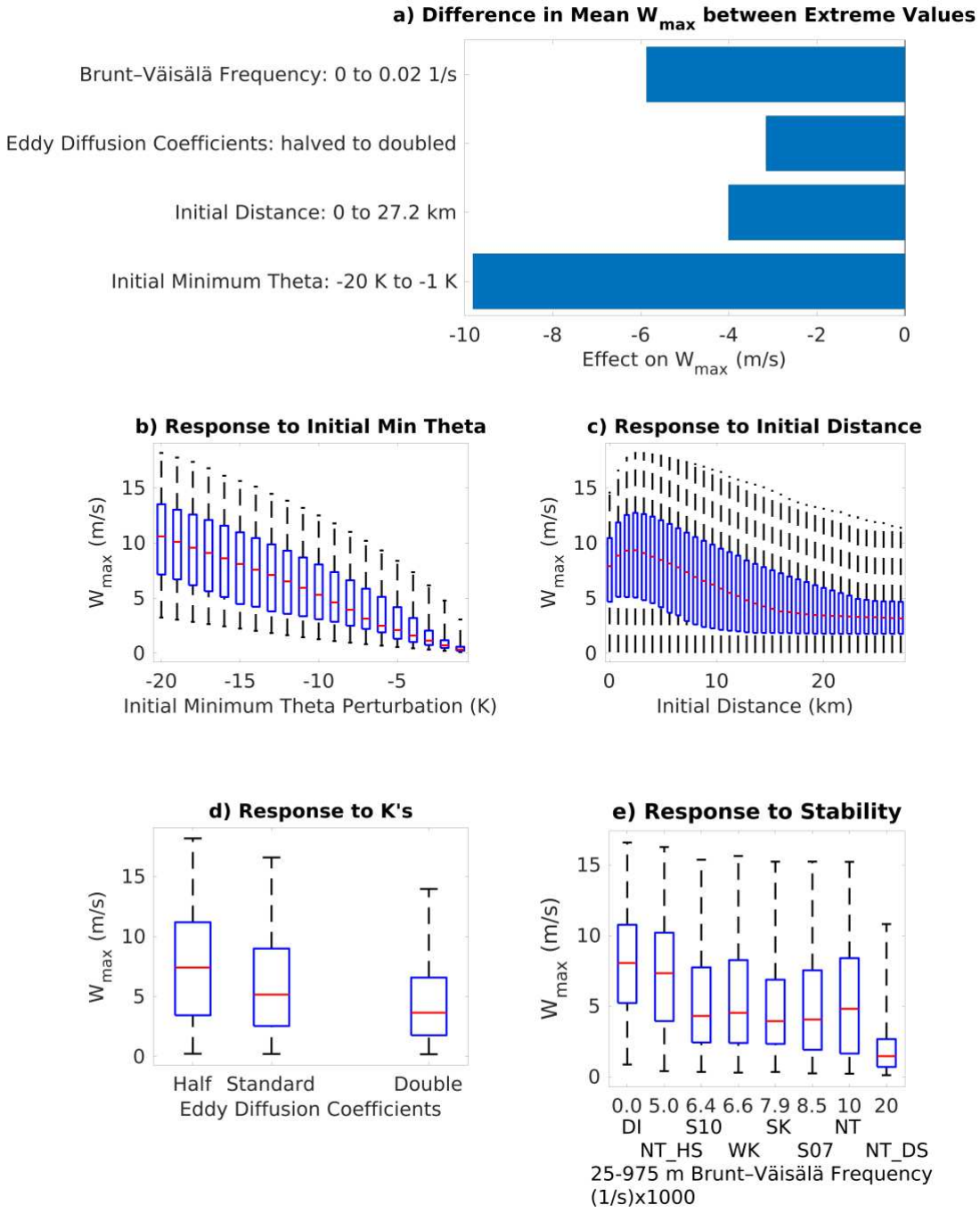

Figure 4.8: Summary of the effects of each parameter tested on the vertical velocity generated as a result of the cold pool collisions. (a) Difference in mean W_max between all simulations with the maximum and minimum tested values of each parameter. Box plots of W_max verses (b) initial temperature perturbation, (c) initial distance, (d) diffusion strength, and (e) low-level static stability. (d) Contains only values from environments where diffusion was varied, and (e) contains only values from simulations with standard diffusion so that the number of points in each box is consistent. Note the abscissa in (e) is non-linear for the sake of clarity.

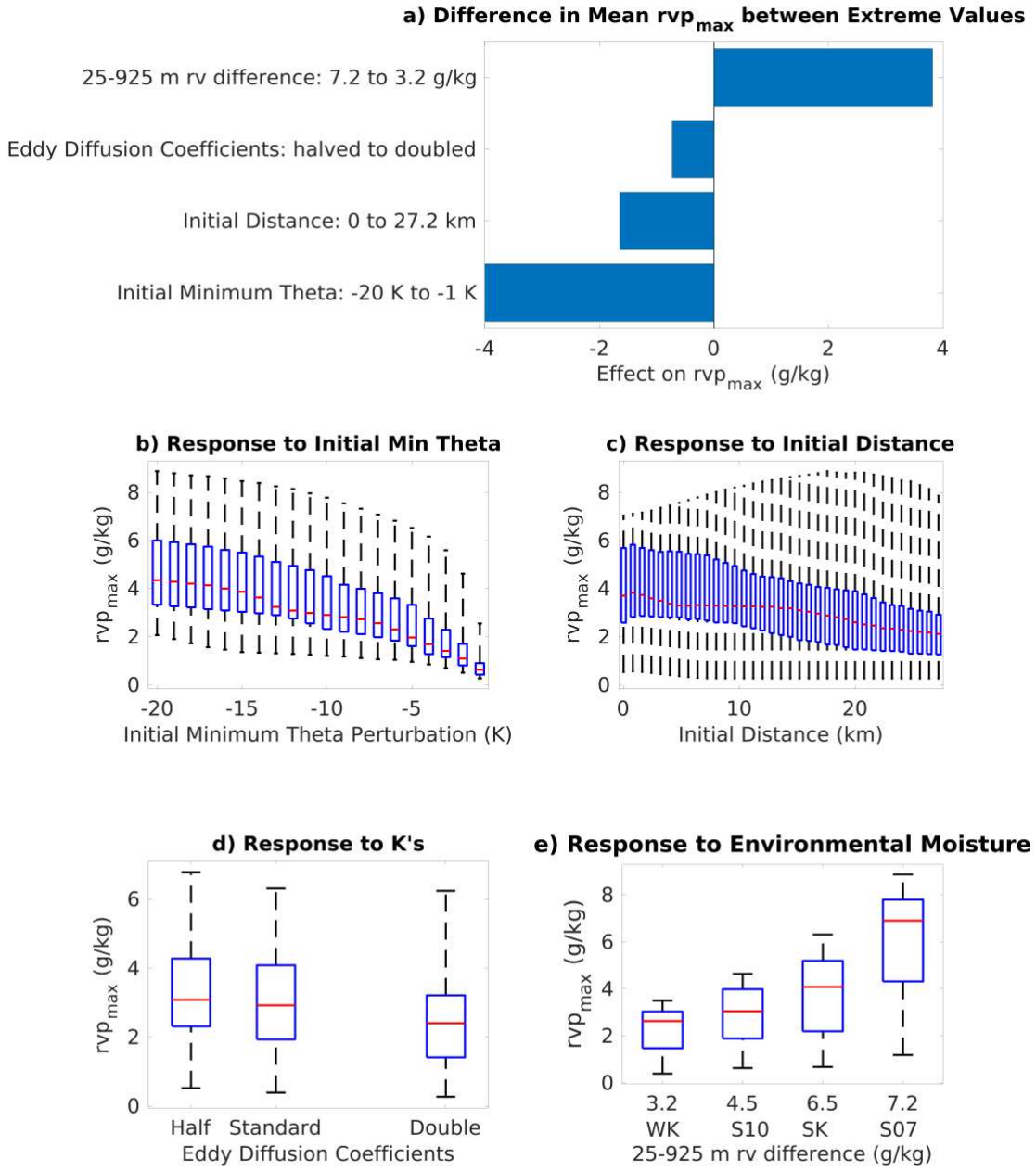

Figure 4.9: Summary of the effects of each parameter tested on the water vapor mixing ratio generated as a result of cold pool collisions. (a) Difference in mean rvp_max between all simulations with the maximum and minimum tested values of each parameter. Box plots of rvp_max verses (b) initial temperature perturbation, (c) initial distance, (d) diffusion strength, and (e) low-level height differential moisture. (d) Contains only values from environments where diffusion was varied, and (e) contains only values from simulations with standard diffusion so

that the number of points in each box is consistent. Note the abscissa in (e) is non-linear for the sake of clarity.

Chapter 5: Conclusions

5.1 Summary of Results

Cold pool collisions are a common process by which new convection can be initiated (Droegemeier and Wilhelmson 1985a,b, Wilson and Schreiber 1986, Lima and Wilson 2008). The objective of this study was to investigate the sensitivity of cold pool collisions to four parameters: (1) the initial cold pool potential temperature perturbations, (2) the initial edge-to-edge distance between the colliding cold pools, (3) the background environment in which the collisions are occurring, and (4) the atmospheric diffusion strength. A large number of 2D, high-resolution ensemble experiments were run using an anelastic non-hydrostatic model to test the impacts of these four parameters on cold pools collisions. Sixteen suites of experiments were conducted. Each suite was comprised of 700 simulations which tested all possible combinations 35 initial cold pool distances and 20 initial cold pool temperature perturbations. The suites varied from each other by having different background environments and/or atmospheric diffusion strength. Water vapor was included in all of the simulations, but was not allowed to condense. To understand the manner in which each of the parameters impacted the ability for cold pool collisions to initiate convection, proxies for mechanical forcing, the maximum vertical velocity (W_max), and for thermodynamic forcing, the maximum water vapor mixing ratio perturbation (rvp_max), were analyzed.

The dynamic and thermodynamic processes driving the cold pool collisions were first thoroughly examined. During a cold pool collision, horizontal convergence from the colliding cold pools was found to increase the near-surface perturbation pressure. This generated a vertical perturbation pressure gradient which drove a strong vertical updraft during the collision. The

updraft advected moisture upwards, leading to enhanced water vapor mixing ratios during the collision. Any process which increased horizontal winds, and thus horizontal convergence, enhanced the vertical velocity and water vapor mixing ratio as a result of the cold pool collision. This upward vertical motion, however, typically lasted only a few minutes due to the fact that some of the lofted air comes from inside the cold pools and is therefore negatively buoyant. In statically stable environments, the vertical gradient in potential temperature contributed to this negative buoyancy as vertical motion advected air of lower potential temperature upwards. In these suites of simulations, in which there were no surface fluxes or condensational processes, a seemingly two-dimensional analog of previously identified cold pool vapor rings (Tompkins 2001) was also created solely through the advection of preexisting moisture.

An assessment of the predominance of the four parameters tested showed that the initial temperature perturbation of the cold pools had the largest impact on the proxies for convective initiation. Cold pools that started colder consistently produced greater W_max and rvp_max than less intense initial cold pools. More intense initial cold pools have more potential energy to convert into kinetic energy. Thus, initially colder cold pools have greater horizontal wind velocities at their heads throughout their lifetimes compared to less intense initial cold pools. Greater horizontal wind velocities produced by initially colder cold pools lead to larger near surface horizontal convergence when these cold pools collide, which drives a faster updraft and larger vertical advection of water vapor, leading to greater W_max and rvp_max.

The second largest impact on the proxies for convective initiation came from the environment in which the cold pools existed. As the low-level static stability, defined as the base state Brunt-Väisälä frequency of the layer from 25 m to 975 m, was increased, W_max arising from the collisions decreased. This decrease in W_max was a result of two effects. The first

effect is increased static stability leading to increased resistance to vertical motion - the aforementioned stabilization effect. Simulations in all environments with a layer of static stability, whether this layer was limited to the surface or extended through the depth of the model domain, had lower domain sum kinetic energy compared to the statically neutral dry isentropic environment. It also seems likely that there is a second effect of gravity waves radiating energy away from the cold pools and thereby dissipating this energy. The effect of low-level static stability was most pronounced for collisions involving cold pools with the smallest initial temperature perturbations (Figure 4.7). Also, as the low-level differential moisture, defined as the base state water vapor mixing ratio at 25 m minus the base state water vapor mixing ratio at 975 m, was increased, rvp_max arising from the collisions increased. This occurred as a result of the vertical advection of base state water vapor. As low-level differential moisture was increased, the magnitude of the vertical gradient of water vapor mixing ratio was increased. Thus, for the same vertical velocity during a cold pool collision, an environment with greater differential moisture generates greater moisture perturbations.

The initial edge-to-edge distance between the cold pools had the third largest impact on the proxies for convective initiation. W_max was found to peak around an optimal initial distance of ~2.5 km, and decreased monotonically for larger or smaller initial distances between cold pools. Analysis of the domain sum kinetic energy elucidated the reason for this peak. Over the lifetime of a pair of cold pools, the domain sum kinetic energy increases at first, because the conversion of potential energy to kinetic energy outpaces the dissipation of kinetic energy. After sufficient time, the domain sum kinetic energy begins to decrease, likely as the dissipation of kinetic energy now occurs at a greater rate than the conversion of potential energy to kinetic energy. Thus, the overall timeseries of domain sum kinetic energy first increases, then peaks,

then finally decreases. Timeseries of horizontal wind velocity maxima also followed this pattern. Cold pools which started closer than the optimal distance collided before horizontal wind velocity would have peaked. Cold pools which started farther than the optimal distance had dissipated significantly before colliding, and thus collided after horizontal wind velocity peaked. W_max was found to decrease in both cases. Cold pools which started at the optimal distance achieved balance between these two effects and thus W_max was maximized. rvp_max peaked at initial distances much larger than the ~2.5 km optimal distance for mechanical forcing. This likely occurs as the faster updraft winds generated during collisions for closely spaced initial cold pools are more effective at advecting moisture away during the collision, thereby decreasing rvp_max.

The parameter which had the smallest effect on the proxies for convective initiation was the atmospheric diffusion rate. Despite its reduced importance, there was a clear relationship between decreased diffusion and increased W_max and rvp_max. Analogous to cold pools with colder initial temperature perturbations, cold pools with decreased diffusion collided when they were colder and thus when they had greater horizontal wind velocities at their heads. This in turn produced greater horizontal convergence and thus greater W_max and rvp_max.

Convective initiation therefore becomes increasingly more likely from a cold pool collision when the cold pools are colder, when the environment is less stable, and when the environment has a greater vertical water vapor gradient. The cold pools starting close to some optimal separation distance and a low atmospheric diffusion rate additionally contribute to an increased chance of convective initiation.

Finally, a classification of cold pool collisions into categories of mechanically and thermodynamically “strong” and “weak” was developed based on the large suite of numerical

experiments conducted. These categories are useful as only strong collisions increase the likelihood of convective initiation beyond that of the action of the individual cold pools. In environments which contained water vapor, thermodynamically strong collisions occurred more frequently than mechanically strong collisions. This suggests that thermodynamic forcing from cold pool collisions may initiate new convection more frequently than mechanical forcing from cold pool collisions.

5.2 Future Work

The results from this research suggest that future work focusing on modeling cold pool collisions, and cold pools in general, should carefully consider the environment chosen. As mentioned before, dry isentropic environments are a common choice in cold pool modeling studies (Liu and Moncrieff 2000, Seigel and van den Heever 2012, Grant and van den Heever 2016, Meyer and Haerter 2020). Cold pools in dry isentropic environments were found to have significantly larger kinetic energy, vertical velocity, and numbers of mechanically strong collisions compared to environments with even minimal stable stratification. Due to these differences, it is recommended that dry isentropic environments are not used when simulating cold pools without comparison to other, more realistic environments. While dissipation of energy by gravity waves is the logical cause of the differences seen in cold pools between dry isentropic and other environments, further study into the cause of these differences should be carried out.

It was shown in this work that peaks in vertical velocity from cold pool collisions are quite fleeting, usually lasting around 5 minutes, while peaks in water vapor mixing ratio generally last somewhat longer. Future work observing and modeling cold pools should therefore strive to use the highest temporal resolution possible. The saving of domain maximum vertical

velocity, domain maximum absolute value of horizontal wind, and domain minimum potential temperature every timestep was beneficial in clearly resolving these peaks.

Given the physically based explanations for the impact of each parameter on mechanical and thermodynamic forcing from cold pool collisions, it is not expected that testing these relationships in three dimensions will qualitatively change results. However, the strength of these relationships could be expected to change in three dimensions, since processes such as the breakdown of Kelvin-Helmholtz waves will be better represented in three dimensions. Testing the impacts of the parameters in three dimensions may therefore provide other further insight.

There remains a vast parameter space to explore regarding cold pools collisions. Grant and van den Heever (2016) found significant impacts of surface fluxes on the dissipation of cold pools. Thus, testing the impact of surface fluxes on cold pool collisions should be conducted. The initial elevation above the surface of cold pools is another interesting factor which should tested in future work. A pair of initially elevated cold pools would theoretically have more time to build kinetic energy, as they would fall vertically first, and then then spread out horizontally and collide. The optimal distance may therefore be reduced in this scenario. Future work should test collisions between asymmetric cold pools. All of the collisions tested in this work were between cold pools which were mirror images of each other. This, however, is somewhat unrealistic and cold pool collisions in the real atmosphere are probably most often between cold pools which differ in age, size, and/or temperature perturbation. Such asymmetries could have a significant impact on the mechanical and thermodynamic forcing from cold pool collisions.

Finally, condensation of water vapor, and thus the formation of deep convection, was excluded in this work in order to keep the simulations simple and efficient to run, and to isolate

the impacts of the collisions on the initial updraft initiated. Future simulations should be performed in which the role of condensed water on convective initiation is investigated.

References

Bukowski, J., and S. C. Heever, 2021: Direct radiative effects in haboobs. *J. Geophys. Res.*, **126**, https://doi.org/10.1029/2021jd034814.

Byers, H. R., and R. R. Braham, 1949: *The Thunderstorm: Report of the Thunderstorm Project*. U.S. Government Printing Office, 287 pp.

Charba, J., 1974: Application of Gravity Current Model to Analysis of Squall-Line Gust Front. *Mon. Weather Rev.*, **102**, 140–156.

Childs, S. J., R. S. Schumacher, and J. L. Demuth, 2020: Agricultural Perspectives on Hailstorm Severity, Vulnerability, and Risk Messaging in Eastern Colorado. *Weather, Climate, and Society*, **12**, 897–911.

Drager, A. J., and S. C. van den Heever, 2017: Characterizing convective cold pools. *J Adv Model Earth Syst*, **9**, 1091–1115.

Droegemeier, K. K., and R. B. Wilhelmson, 1985a: Three-Dimensional Numerical Modeling of Convection Produced by Interacting Thunderstorm Outflows. Part II: Variations in Vertical Wind Shear. *J. Atmos. Sci.*, **42**, 2404–2414.

——, and ——, 1985b: Three-dimensional numerical modeling of convection produced by interacting thunderstorm outflows. Part I: Control simulation and low-level moisture variations. *Journal of Atmospheric Sciences*, **42**, 2381–2403.

Engerer, N. A., D. J. Stensrud, and M. C. Coniglio, 2008: Surface Characteristics of Observed Cold Pools. *Mon. Weather Rev.*, **136**, 4839–4849.

Feng, Z., S. Hagos, A. K. Rowe, C. D. Burleyson, M. N. Martini, and S. P. Szoeke, 2015: Mechanisms of convective cloud organization by cold pools over tropical warm ocean during the AMIE/DYNAMO field campaign. *Journal of Advances in Modeling Earth Systems*, **7**, 357–381.

Goff, R. C., 1976: Vertical Structure of Thunderstorm Outflows. *Mon. Weather Rev.*, **104**, 1429–1440.

Grant, L. D., and S. C. van den Heever, 2016: Cold pool dissipation. *Journal of Geophysical Research Atmospheres*, **121**, 1138–1155.

——, and ——, 2018: Cold pool-land surface interactions in a dry continental environment. *J Adv Model Earth Syst*, **10**, 1513–1526.

——, T. P. Lane, and S. C. van den Heever, 2018: The Role of Cold Pools in Tropical Oceanic Convective Systems. *J. Atmos. Sci.*, **75**, 2615–2634.

Houston, A. L., and R. B. Wilhelmson, 2011: The Dependence of Storm Longevity on the Pattern of Deep Convection Initiation in a Low-Shear Environment. *Mon. Weather Rev.*, **139**, 3125–3138.

Huppert, H. E., and J. E. Simpson, 1980: The slumping of gravity currents. *J. Fluid Mech.*, **99**, 785-799.

Intrieri, J. M., A. J. Bedard, and R. M. Hardesty, 1990: Details of Colliding Thunderstorm Outflows as Observed by Doppler Lidar. *J. Atmos. Sci.*, **47**, 1081–1099.

Kingsmill, D. E., 1995: Convection Initiation Associated with a Sea-Breeze Front, a Gust Front, and Their Collision. *Mon. Weather Rev.*, **123**, 2913–2933.

Langer, G., G. Morgan, C. T. Nagamoto, M. Solak, and J. Rosinski, 1979: Generation of Ice Nuclei in the Surface Outflow of Thunderstorms in Northeast Colorado. *J. Atmos. Sci.*, **36**, 2484–2494.

Langhans, W., and D. M. Romps, 2015: The origin of water vapor rings in tropical oceanic cold pools. *Geophysical Research Letters*, **42**, 7825–7834.

Lima, M. A., and J. W. Wilson, 2008: Convective Storm Initiation in a Moist Tropical Environment. *Mon. Weather Rev.*, **136**, 1847–1864.

Liu, C., and M. W. Moncrieff, 1996: A Numerical Study of the Effects of Ambient Flow and Shear On Density Currents. *Mon. Weather Rev.*, **124**, 2282–2303.

——, and ——, 2000: Simulated Density Currents in Idealized Stratified Environments. *Mon. Weather Rev.*, **128**, 1420–1437.

McNulty, R. P., 1995: Severe and Convective Weather: A Central Region Forecasting Challenge. *Weather Forecast.*, **10**, 187–202.

Meyer, B., and J. O. Haerter, 2020: Mechanical Forcing of Convection by Cold Pools: Collisions and Energy Scaling. *J Adv Model Earth Syst*, **12**, e2020MS002281.

Miller, S. D., A. P. Kuciauskas, M. Liu, Q. Ji, J. S. Reid, D. W. Breed, A. L. Walker, and A. A. Mandoos, 2008: Haboob dust storms of the southern Arabian Peninsula. *J. Geophys. Res.*, **113**, https://doi.org/10.1029/2007jd008550.

Parker, M. D., 2007: Simulated Convective Lines with Parallel Stratiform Precipitation. Part II: Governing Dynamics and Associated Sensitivities. *J. Atmos. Sci.*, **64**, 289–313.

Purdom, J. F. W., 1976: Some Uses of High-Resolution GOES Imagery in the Mesoscale Forecasting of Convection and Its Behavior. *Mon. Weather Rev.*, **104**, 1474–1483.

——, 1982: Subjective interpretations of geostationary satellite data for nowcasting. *Nowcasting*, K.A. Browning, Ed., Academic Press, 149–166.

Reid, J. S. and coauthors, 2021: The coupling between tropical meteorology, aerosol science, convection and the energy budget during the Clouds, Aerosol Monsoon Processes Philippines Experiment (CAMP2Ex). To be submitted to *Bull. Am. Meteorol. Soc.*

Roberts, A., and P. Knippertz, 2012: Haboobs: convectively generated dust storms in West Africa. *Weather,* **67**, 311-316.

Rotunno, R., J. B. Klemp, and M. L. Weisman, 1988: A Theory for Strong, Long-Lived Squall Lines. *J. Atmos. Sci.*, **45**, 463–485.

Schlemmer, L., and C. Hohenegger, 2016: Modifications of the atmospheric moisture field as a result of cold-pool dynamics. *Quart. J. Roy. Meteor. Soc.*, **142**, 30–42.

Seigel, R. B., and S. C. van den Heever, 2012: Simulated Density Currents beneath Embedded Stratified Layers. *J. Atmos. Sci.*, **69**, 2192–2200.

Simpson, J. E., 1969: A comparison between laboratory and atmospheric density currents. *Quart. J. Roy. Meteor. Soc.*, **95**, 758–765.

Simpson, J. E., 1972: Effects of the lower boundary on the head of a gravity current. *J. Fluid Mech.*, **53**, 759–768.

——, 1997: *Gravity Currents*. Cambridge University Press, 244 pp.

Sokolowsky, G. A., S. W. Freeman, and S. C. van den Heever, 2021: Sensitivities of Maritime Tropical Trimodal Convection to Aerosols and Boundary Layer Static Stability. In review at *J. Atmos. Sci.*

Thiery, W., E. L. Davin, S. I. Seneviratne, K. Bedka, S. Lhermitte, and N. P. M. van Lipzig, 2016: Hazardous thunderstorm intensification over Lake Victoria. *Nat. Commun.*, **7**, 12786.

Tompkins, A. M., 2001: Organization of Tropical Convection in Low Vertical Wind Shears: The Role of Cold Pools. *J. Atmos. Sci.*, **58**, 1650–1672.

Torri, G., and Z. Kuang, 2016: Rain evaporation and moist patches in tropical boundary layers. *Geophys. Res. Lett.*, **43**, 9895–9902.

——, and ——, 2019: On cold pool collisions in tropical boundary layers. *Geophys. Res. Lett.*, **46**, 399–407.

——, ——, and Y. Tian, 2015: Mechanisms for convection triggering by cold pools. *Geophys. Res. Lett.*, **42**, 1943–1950.

Trier, S. B., W. C. Skamarock, M. A. LeMone, D. B. Parsons, and D. P. Jorgensen, 1996: Structure and Evolution of the 22 February 1993 TOGA COARE Squall Line: Numerical Simulations. *J. Atmos. Sci.*, **53**, 2861–2886.

Weaver, J. F., and S. P. Nelson, 1982: Multiscale Aspects of Thunderstorm Gust Fronts and Their Effects on Subsequent Storm Development. *Mon. Weather Rev.*, **110**, 707–718.

Weckwerth, T. M., and R. M. Wakimoto, 1992: The Initiation and Organization of Convective Cells atop a Cold-Air Outflow Boundary. *Mon. Weather Rev.*, **120**, 2169–2187.

Weisman, M. L., and J. B. Klemp, 1982: The Dependence of Numerically Simulated Convective Storms on Vertical Wind Shear and Buoyancy. *Mon. Weather Rev.*, **110**, 504–520.

Weisman, M. L., and R. Rotunno, 2004: "A Theory for Strong Long-Lived Squall Lines" Revisited. *J. Atmos. Sci.*, **61**, 361–382.

Wilson, J. W., and W. E. Schreiber, 1986: Initiation of Convective Storms at Radar-Observed Boundary-Layer Convergence Lines. *Mon. Weather Rev.*, **114**, 2516–2536.

——, and D. L. Megenhardt, 1997: Thunderstorm Initiation, Organization, and Lifetime Associated with Florida Boundary Layer Convergence Lines. *Mon. Weather Rev.*, **125**, 1507–1525.

Zipser, E. J., D. J. Cecil, C. Liu, S. W. Nesbitt, and D. P. Yorty, 2006: WHERE ARE THE MOST INTENSE THUNDERSTORMS ON EARTH? *Bull. Am. Meteorol. Soc.*, **87**, 1057–1072.